A multibody simulation approach to identify critical instability scenarios of a forklift truck

Jhala, Harditya S.

Award date:
2023

Department of Mechanical Engineering
Dynamics and Control

Master Automotive Technology

A multibody simulation approach to identify critical instability scenarios of a forklift truck

Master thesis

H.S.Jhala (1693611) [h.s.jhala@student.tue.nl]

DC 2023.076

Internal Supervisor:
dr. ir. I.J.M. Besselink

External Supervisor:
Pantelis Nikolaou, Msc. [Hyster-Yale Group]

This report was made in accordance with the TU/e Code of Scientific Conduct for the Master thesis.

Eindhoven, 28 September 2023

Acknowledgments

I would like to express my sincere gratitude to the people who have supported and motivated me while I was pursuing my graduation project at the Technical University of Eindhoven.

First and foremost, I would like to thank my university supervisor, dr. ir. Igo Besselink, who provided me with the guidance and direction to achieve the outcome obtained in this master thesis. Dr. Besselink was always keen on my progress and consistently displayed eagerness to teach me the concepts relevant to the challenges I encountered while carrying out my project. In our weekly meetings, his insightful feedback and thoughtful comments helped me to fully understand what I have implemented and sparked my interest in carrying forward the research I executed in vehicle dynamics.

I would also like to express my gratitude to Pantelis Nikolaou, MSc., who functioned as my supervisor at Hyster-Yale Group. Pantelis was always available to solve my doubts and gave me insights related to my master thesis. His unwavering support and constant encouragement were instrumental in my success. Pantelis also emphasized the importance of taking breaks and maintaining a healthy work-life balance during challenging times, which was invaluable advice.

Special thanks to Neha Roy for providing me with the opportunity to pursue my internship and graduation project at Hyster-Yale Group. I would also like to express my gratitude to the test engineers for helping me conduct various tests despite their busy schedules. Special thanks to Maiko Buurman who showed interest in my master thesis and was available for discussions which led to interesting solutions.

Finally, I would like to thank my family and friends for believing in me throughout this journey. Their emotional support, love and affection were the pillars that sustained me during the highs and lows of this endeavor.

Abstract

Identifying stability limits for heavy-duty forklift trucks has always been challenging. The probability of bringing the truck into an unstable situation is notably high due to elevated lift heights resulting in a high vertical center of gravity. This increases the susceptibility of forklifts to tip or roll over if driven with a lack of awareness. While striving to identify the stability limits of a forklift, computer simulation technology has proven to be pivotal, where full vehicle simulation models are being used. The purpose of this study is to develop a parameterized multibody model for the Hyster forklift H9XD6 to identify critical instability scenarios and ascertain the stability thresholds of the truck. The outcomes of this research can be used to contribute to the development of warning systems, thereby elevating driver awareness and enhancing overall operational safety.

A multibody model of the forklift is developed in MATLAB Simulink, utilizing the Simscape multibody toolbox. Subsystems such as chassis, front axle, rear axle and front-end assembly of a forklift are modeled by connecting rigid bodies with various joints to represent the actual vehicle. Subsystems such as engine, transmission, steering system and brakes are modeled in a simplified way as they are insignificant from a stability prediction point of view.

Following the model's development, a validation process is executed, commencing with straightforward tests to confirm the accuracy of output signals in terms of magnitude and sign. The validation procedure consists of two stages. First, static tests are conducted to compare the CoG locations of the forklift at different lift heights. Further, the ISO 22915 stability tests are simulated in the virtual environment. Lastly, dynamic tests are conducted to observe both steady-state and dynamic response of the model and signals are compared with measurements. To get an idea of how well the model represents reality, an accuracy criterion consisting of various correlation coefficients is established. Based on the results obtained, a well-validated multibody forklift model is created, which can be used to identify critical scenarios of instability.

Based on day-to-day situations that a forklift driver may encounter, four critical scenarios which bring the forklift into an unstable condition have been simulated. Based on the stability metrics, a point of criticality is identified when the forklift reaches operational limits within each scenario. Values of parameters such as critical velocity and accelerations are determined above which the forklift should not operate for that particular scenario. These insights help to evaluate the stability limits of a forklift truck, aiding the development of advanced warning systems and operational safety enhancement. The developed multibody model is capable of representing other truck variants by altering parameters.

Contents

Acknowledgements **i**

Abstract **ii**

Nomenclature **v**

1 Introduction **1**
1.1 Background . . . 1
1.2 Research questions & objectives . . . 2
1.3 Contributions . . . 3
1.4 Report outline . . . 3

2 Literature Review **5**
2.1 Stability concepts . . . 5
2.2 ISO 22915 regulations: verification of stability . . . 7
2.3 Multibody modeling . . . 9
2.4 Identifying critical instability scenarios . . . 9
2.5 Summary . . . 10

3 Dynamics of a rear-wheel steered vehicle **11**
3.1 Instantaneous center of rotation . . . 11
3.2 Dual steer bicycle model . . . 13
3.3 Summary . . . 16

4 Multibody Forklift Model **17**
4.1 Model overview . . . 17
4.2 Model implementation . . . 19
4.3 Summary . . . 26

5 Model Simulation & Validation **27**
5.1 Static validation . . . 27
5.2 ISO 22915: verification of stability tests . . . 28
5.3 Validation using dynamic tests . . . 31
5.4 Summary . . . 38

6 Identification of Critical Scenarios **39**
6.1 Critical scenario 1: Approaching a stack . . . 40
6.2 Critical scenario 2: Stack exit . . . 41
6.3 Critical scenario 3: Ramp steer response . . . 43
6.4 Critical scenario 4: 90 degree turn . . . 44

6.5 Boundary conditions 45

7 Conclusions & Recommendations **47**
7.1 Conclusions 47
7.2 Recommendations 49

References **50**

A Model Simulation guide **52**
A.1 Run: ISO 22915 verification of stability tests 53
A.2 Run: Dynamic validation tests 53

B Accelerometer modelling **54**

C Multibody model validation results **57**
C.1 ISO 22915: verification of stability 57
C.2 Steady-state circular driving: right turn 61

Nomenclature

Symbols

Symbol	Description	Unit
α_{st}	Angle to denote forward stability	deg.
$\alpha_{st\_\text{threshold}}$	Threshold angle for forward stability	deg.
β_{st}	Angle to denote lateral stability	deg.
$\beta_{st\_\text{threshold}}$	Threshold angle for lateral stability	deg.
F_{x_CoG}	Longitudinal force acting on CoG	N
F_{y_CoG}	Lateral force acting on CoG	N
$F_{z\text{Front}}$	Vertical force on the front tires	N
$F_{z\text{Rear}}$	Vertical force on the rear tires	N
a_x	Longitudinal acceleration	m/s^2
a_y	Lateral acceleration	m/s^2
g	Acceleration due to gravity	m/s^2
m	Mass of the truck	kg
R	Pearson's correlation coefficient	–
ϵ	Offset error	–
v	Lateral velocity	m/s
r	Yaw velocity	deg./s
δ_1	Front Steering angle	deg.
δ_2	Rear Steering angle	deg.
α_1	Front side slip angle	deg.
α_2	Rear side slip angle	deg.
β	Vehicle side slip angle	deg.
F_{y1}	Front tire lateral force	N
F_{y2}	Rear tire lateral force	N
l	wheelbase	m
C	Instantaneous center of rotation	–
R	Vehicle turning radius	m
I_{zz}	Yaw moment of inertia	kgm^2
a	Distance to CoG from front axle	m
b	Distance to CoG from rear axle	m
C_1	Front tire cornering stiffness	N/rad
C_2	Rear tire cornering stiffness	N/rad
u	Longitudinal velocity	m/s
x	State vector	–
u	Input vector	–
y	Output vector	–

Symbol	Description	Unit
$V_{x\text{Low}}$	Lower Boundary velocity in slip calculation	m/s
F	Actuator force for the bushing joint	N
x	Displacement/deflection at tire contact patch	m
$\dot{x}$	Sliding velocity at tire contact patch	m/s
b_{damp}	Damping coefficient	Ns/m
V_{sx}	Sliding longitudinal velocity	m/s
V_{sy}	Sliding lateral velocity	m/s
F_z	Vertical force on tire	N
K_x	Longitudinal stiffness	N/m
K_y	Lateral stiffness	N/m
K_z	Vertical stiffness	N/m
T_{engine}	Engine torque	Nm
T_{out}	Torque on driven wheels	Nm
τ_{throttle}	Throttle pedal position	–
P_{engine}	Engine power	kW
ω_{wheel}	Angular velocity at the wheels	rad/s
ω_{engine}	Angular velocity at engine output shaft	RPM
i_1	First gear ratio	–
i_{fd}	Final drive ratio	–
T_{limitor}	Torque limiter	–
$M_{b,\text{max}}$	Maximum brake torque	Nm
r_t	Radius of tire	m
μ	Coefficient of friction	–
F_x	Longitudinal force on tire	N
$F_{z,\text{FA}}$	vertical force on the front axle	N
θ	Stability platform angle	deg.
$\vec{f}$	Measured resultant acceleration on IMU	m/s^2
$\vec{a}$	Measured resultant acceleration by transform sensor	m/s^2
$\vec{g}$	Gravitational acceleration vector	m/s^2
$a_{x,\text{IMU}}$	Longitudinal acceleration measured by IMU	m/s^2
$a_{y,\text{IMU}}$	Lateral acceleration measured by IMU	m/s^2
$a_{z,\text{IMU}}$	Vertical acceleration measured by IMU	m/s^2
$a_{x,\text{sensor}}$	Longitudinal acceleration measured by sensor	m/s^2
$a_{y,\text{sensor}}$	Lateral acceleration measured by sensor	m/s^2
$a_{z,\text{sensor}}$	Vertical acceleration measured sensor	m/s^2
r_{ii}	Rotational component along the ii axis	–
x_{i}	i_{th} element of the measured output	–
y_{i}	i_{th} element of the simulated output	–
$\bar{x}$	mean value of the measured output	–
$\bar{y}$	mean value of the simulated output	–
n	number of samples	–
δ_{tire}	tire angle	deg.
V_x	Vehicle forward velocity	km/h

Symbol	Description	Unit
RI	Rollover Index	–
$F_{z\text{Left}}$	Combined vertical force on left side	N
$F_{z\text{Right}}$	Combined vertical force on right side	N
TI	Tipover Index	–
T_{pivot}	Torque at the rear axle to stop pivot motion	Nm
θ_{pivot}	Pivot angle for rear axle	deg.
δ_{right}	Right tire angle	deg.
δ_{left}	Left tire angle	deg.
$\delta_{\text{SteeringWheel}}$	Steering wheel angle	deg.
δ_{tire}	Tire angle	deg.
τ_{brake}	Brake pedal position	–
t	Time	s
s	value of slope in % used in ISO 22915 stability tests	–
ϕ	Vehicle roll angle	deg.
R^*	Rotation matrix	–

Glossary

Acronym	Description
CAD	Computer Aided Design
CAN	Controller Area Network
CoG	Center of Gravity
FEE	Front End Equipment
HCG	Center of Gravity coordinate in x-direction
IC	Instantaneous Center
IMU	Inertial Measurement Unit
ISO	International Organisation for Standardization
LLTR	Lateral Load Transfer Ratio
MF	Magic Formula
MLH	Maximum Lift Height
NRMSD	Normalised Root Mean Square Deviation
ODE	Ordinary Differential Equation
PI	Proportional Integral
RI	Rollover Index
RPM	Rotation per Minute
TARS	Transportation Attitude Reference Sensor
TI	Tipover Index
ULT	Ultimate
VCG	Center of Gravity coordinate in z-direction
WL	Wheel Lift
WWRP	World Wide Rating Program

Chapter 1

Introduction

1.1 Background

Forklift trucks are heavy-duty vehicles that are widely used by construction, manufacturing, and shipping industries to undertake their day-to-day activities of transportation. A forklift truck is differentiated from all other trucks based on the front end that is used to lift and carry heavy objects. Figure 1.1 shows the Hyster forklift H9XD6 equipped with the front end assembly primarily comprising of mast, carriage and forks. Component (1) shown in Figure 1.1 is known as a mast, which is used to reach the desired height to position or lift the payload. The mast is connected to the chassis and can also be tilted in the forward or backward direction. Generally, the mast is back-tilted to ensure safety when the truck is driving while carrying a heavy load. Components (2) and (3) are known as carriage and forks, respectively. Carriage is used to link the forks with the mast and gives the possibility to side shift the forks. The two forks can be side shifted depending on the size of the object or a pallet to be carried. This way, the front-end equipments are used collectively to lift and transport containers and heavy pallets.

According to a survey conducted in the USA, there is a 90% probability that a lift truck is involved in an accident over its useful lifetime [1]. Also, data presented regarding the type of accidents concerning forklift fatalities shows that 42% of the total accidents are caused by tipping/rolling over of a forklift. To enhance safety and reliability and lower forklift fatalities, research is being conducted to identify stability limits of a lift truck.

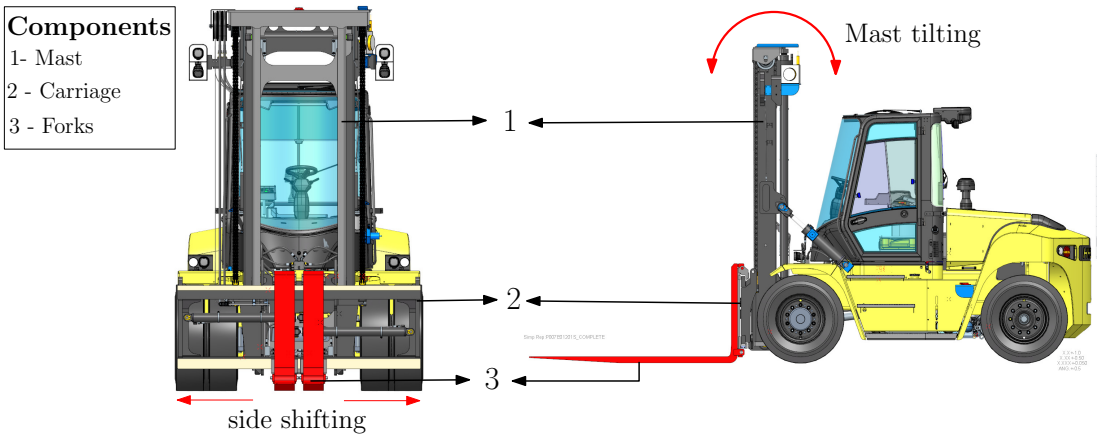

Figure 1.1: Hyster forklift H9XD6

Unfortunately, conducting physical tests to determine the stability limit of a lift truck poses considerable challenges and safety concerns. As a result, researchers aim to predict the behavior and establish the stability limits of lift trucks through the development of virtual tools utilizing computer simulation technology. Developing a tool capable of predicting the behavior of a heavy-duty vehicle within a virtual environment can serve multiple purposes, saving valuable resources such as time, effort, and capital invested in vehicle testing. Most importantly, a validated virtual tool can effectively determine the stability limits of a lift truck, whose surpassing often leads to hazardous accidents. Once the stability limits are determined virtually, they can be used to develop a warning system for drivers to prevent accidents. Beyond their application in warning systems, this information can also serve as an input to develop control systems that prevent such dangerous situations.

1.2 Research questions & objectives

The International Organization for Standardization (ISO) has established the ISO 22915 verification of stability tests [2], outlining a forklift's stability limits. These tests primarily rely on steady-state calculations, not accounting for sudden dynamic maneuvers that involve transient responses. The stability limits indicated by ISO 22915 tests may not be applicable for sudden dynamic maneuvers, potentially leading to truck instability before reaching the ISO results. Therefore, a trustworthy virtual tool is required for predicting vehicle behavior in steady state as well as dynamic situations. Moreover, it is also important to know what the critical scenarios are that can cause unstable behavior of the forklift. To address these concerns, the two research questions answered in this study are formulated as follows: "*How can we predict the stability limits of a forklift in dynamic conditions within a virtual environment?*" and "*What are the critical real-life situations which might result in unstable behavior of the lift truck?*".

To address the formulated research questions regarding the stability limits for forklifts, distinct objectives are outlined:

- Model a fully functional parameterised multibody model of the forklift H9XD6 with subsystems such as chassis, front axle, rear axle and front end equipment.
- Model the auxiliary subsystems such as engine, transmission, braking system and steering system mathematically utilizing Simulink. This approach is preferred as these subsystems do not directly influence the project goal and can be simplified.
- Execute a comprehensive vehicle validation program comprising of both static and dynamic testing maneuvers.
- Simulate the ISO 22915 verification of stability tests for the Hyster forklift H9XD6.
- Simulate the validated multibody model under various critical scenarios that may induce truck instability.
- Observe the simulation outputs of the critical scenarios and identify parameters such as critical velocity and accelerations above which the truck exhibits instability.

After achieving the above listed objectives, the virtual prediction of vehicle behavior is achieved and stability limits of a forklift truck are identified for different situations.

1.3 Contributions

The primary contribution of this research lies in the development of a multibody model for the forklift truck, capable of simulating various scenarios that are challenging to replicate through real-world vehicle testing due to associated risks. After simulating critical situations, boundary conditions are identified which provide upper bounds to various parameters beyond which the truck exhibits instability.

The parameterized model can be utilized for simulating the static stability platform tests imposed by ISO [2]. Every truck must meet the forward and lateral stability test requirements determined by ISO to be operated commercially. At present, lift trucks are positioned on a stability platform, and tilt tests are performed by restricting the truck from tipping/rolling over by external methods. Consequently, these tests demand an expensive infrastructure along with a significant risk factor for an uncertain calamity.
In this study, the ISO 22915 stability tests are simulated for the forklift H9XD6, yielding promising results. Therefore, by altering vehicle parameters, these tests can be performed for every truck by virtual computer simulation. This would result in lowering the resources and efforts invested in conducting physical vehicle testing.

Since the modeled forklift is rear-wheel steered, the dynamics of a rear wheel steered vehicle are studied in this research. The equations of motion and state space representation for a dual steer bicycle model are formulated to observe the yaw dynamics for a rear-wheel steered vehicle. Since the steered wheels for such a vehicle turn in the opposite direction compared to the direction of turning, the lateral force developed by the steered rear tire initially develops in the opposite direction of the turn. This leads to the lateral acceleration building in the opposite direction as well towards the start of the corner. However, since the yaw rate of the vehicle irrespective of being front or rear wheel steered vehicle is same, the lateral force and acceleration eventually change sign for a rear wheel steered vehicle. A theoretical explanation for the yaw dynamics is presented in the thesis.

1.4 Report outline

Based on the research questions and objectives described in Section 1.2, this research focuses on developing a multibody model of a forklift truck that can be used to identify critical instability scenarios. Chapter 2 provides insight into the stability concepts used in the forklift industry and explains different approaches to develop a multibody model. Along with stability concepts and modeling aspects, this chapter also discusses some metrics which are used to identify unstable situations. Chapter 3 discusses the unique handling characteristics of a rear-wheel steered vehicle, which are validated by using the single track vehicle model, also known as bicycle model. The bicycle model is modified to include dual steering and effect of rear wheel steering on yaw dynamics is investigated in this chapter. Chapter 4 discusses the forklift multibody model development approach and gives insight into the modeling aspects and integration of each subsystem. Chapter 5 presents several validation tests performed to access the accuracy of the developed model along with discussing the testing equipment and environment. Chapter 6 presents four critical scenarios simulated using the multibody model. Information about stability limits and critical values for various parameters above which the truck exhibits instability have been determined. Chapter 7 discusses the conclusions drawn from this research and presents recommendations for enhancing the model and stability results in the future.

Chapter 2

Literature Review

This chapter provides a literature review related to the important aspects covered in this thesis. Since the research is related to identifying critical instability scenarios, stability concepts of a lift truck are discussed in the first section. These stability concepts are a foundation for the ISO 22915 verification of stability standards for industrial trucks [2]. Subsequently, the stability tests formulated under the ISO 22915 standards are illustrated in Section 2.2, which account for the stability margins of the lift truck. In Section 2.3, several studies on multibody modeling are discussed, which are utilized to build a fully functional forklift multibody model. The section also includes literature on model validation and quantifying the level of agreement between the measurements and the model results. Finally, to identify unstable situations, several metrics are classified in Section 2.4, which indicate initiation of a tip over in the longitudinal and lateral direction.

2.1 Stability concepts

The concept of stability triangle is a general concept which indicates a forklift's stability explained in the literature by Mohamed [3]. The stability triangle refers to the triangle formed by the front axle and the imaginary lines drawn from the center points of the front tires to the center of the rear axle, projected on the ground, as shown in Figure 2.1 [3].

The concept of stability triangle indicates two types of stability, namely: forward stability and lateral stability. The resistance of the forklift to tip over in the forward direction is known as the forward stability, whereas, the resistance of a forklift to roll sideways, is known as the lateral stability. The truck's resistance to tip or roll over is determined by the position of the combined CoG of the truck including the payload relative to the boundaries of the stability triangle [4]. The forward stability of a forklift truck is governed by line AB in Figure 2.1, which depicts the front axle of the truck. If the CoG lies outside the front boundary of the stability triangle, there is a high possibility for the truck to tip over in the forward direction [4]. Lateral stability is governed by the CoG position of the truck relative to the two sides of the stability triangle AC and BC, as shown in Figure 2.1.

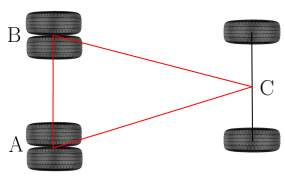

Figure 2.1: Stability triangle for a lift truck

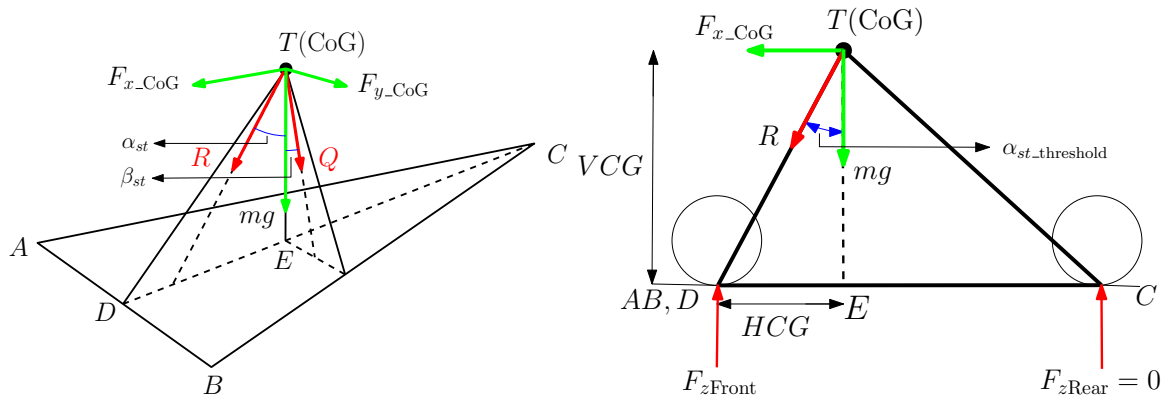

(a) Isometric View **(b)** Side view

Figure 2.2: Longitudinal and lateral resultant forces on the CoG: Stability triangle [5].

Moreover, there is a trade-off between the forward and the lateral stability of a forklift truck. When the CoG is shifted backward, the forward stability increases, however, the lateral stability decreases due to the narrowing boundaries of the stability triangle [5].

According to Pantelis Nikolaou [5], the stability triangle can also be used for identifying the initiation of tipping/rolling over of a truck in steady-state driving situations. Considering a longitudinal braking situation, the action line of the resultant force R, shown in Figure 2.2a, acting at the CoG of the truck should meet the ground surface within the stability triangle ABC. Similarly, for a cornering situation, the action line of the resultant force Q, also shown in Figure 2.2a, formed by the vectorial addition of lateral force (F_{y_CoG}) and the gravitational force (mg) should be within the stability triangle to remain stable.

The angles α_{st} and β_{st} shown in Figure 2.2a are of great importance to identify the initiation of tipping and rolling over in dynamic situations. In case of braking, when the rear axle reaction force becomes zero, the action line of the resultant force R points exactly to line AB as shown in Figure 2.2b [5]. At this instant, the truck will start to tip in the forward direction. In this condition, the angle formed between the line TD and TE is the threshold angle for forward stability ($\alpha_{st\_\text{threshold}}$). As soon as the resultant braking force which is the vectorial addition of the longitudinal force (F_{x_CoG}) and the gravitational force (mg) meets the ground outside the stability triangle, the truck can tip. Therefore, the maximum longitudinal acceleration at the CoG of a lift truck should always be less than the product of gravitational acceleration and the tangent of ($\alpha_{st\_\text{threshold}}$) for the truck to remain stable [5]. This is shown in (2.1). The same concept is also applicable considering the angle β_{st} to account for lateral stability, which is given by (2.2).

$$a_x \leq g \tan(\alpha_{st\_\text{threshold}}), \tag{2.1}$$

$$a_y \leq g \tan(\beta_{st\_\text{threshold}}), \tag{2.2}$$

where a_x, a_y and g are the longitudinal, lateral and gravitational acceleration, respectively.

Hence, the angles α_{st} and β_{st} denote the forward and lateral stability margins of the truck, respectively. The main takeaway for the stability triangle concept is that the resultant force acting on the CoG of the truck should meet the ground surface inside the stability triangle which will keep the respective α_{st} and β_{st} smaller than the respective threshold values. The theory and derivations can be found in the work of Nikolaou [5].

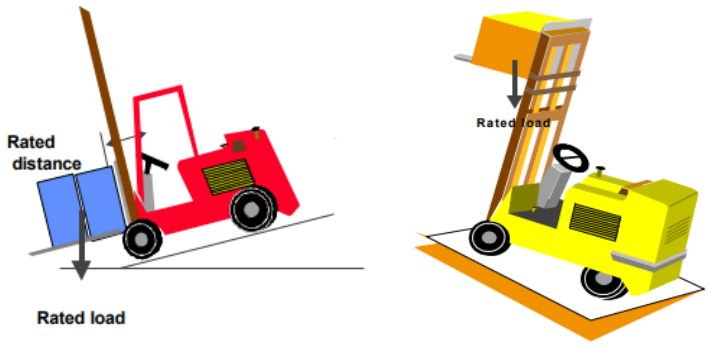

(a) Test 2: Forward Stability **(b)** Test 3: Lateral Stability

Figure 2.3: ISO 22915 regulations: verification of stability

2.2 ISO 22915 regulations: verification of stability

ISO has developed tests, that use the concepts of the stability triangle for the verification of the stability of a forklift truck. These tests are formulated to approximate the $\alpha_{st\_\text{threshold}}$ and $\beta_{st\_\text{threshold}}$ angles of the truck and compare the identified angles to a minimum standard. The truck is only allowed to be operated commercially if it is stable at these minimum stability limits. ISO 22915-2 [2] verification of stability consists of four tests for counterbalance trucks with masts, two for forward and two for lateral stability. The tilt tests for the forward and lateral stability of the truck are conducted by using a tilt platform, known as a tilt table, as shown in Figure 2.3. The standard tests specified under ISO 22915-2 verification of stability are summarised below.

Test 1/2: Forward Stability

The truck is positioned on the tilt platform such that the load axle CC of the truck is parallel to the tilt axis XY, as shown in Figure 2.4a. The rated payload is placed on the forks of the truck and the mast is shifted to the highest position. Due to rated load elevated at the maximum height, point E shown in Figure 2.4b, on the front face of the forks shifts forward. To make sure that point E is again realigned to the same position, the mast is back-tilted as shown in Figure 2.4b. The amount by which the mast is back tilted is determined experimentally. After the truck is positioned according to the rules, the platform is tilted about the XY axis and the tilt angle at which the reaction force on the rear axle becomes 0 is noted. This denotes the angle $\alpha_{st\_\text{threshold}}$ at which the truck initiates to tip forward.

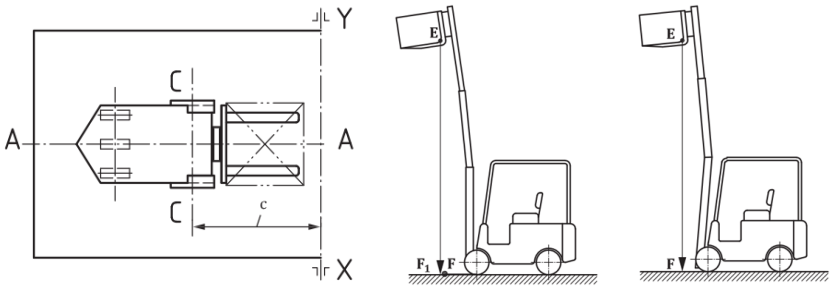

(a) **(b)**

Figure 2.4: ISO 22915 regulations: verification of stability. Test 1: Forward Stability [2]

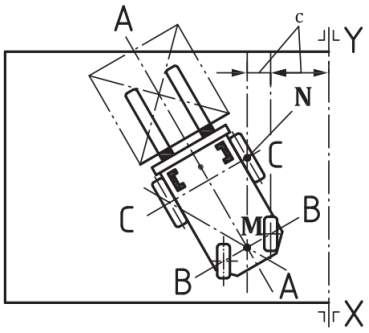

Figure 2.5: Top view depicting roll axis parallel to the tilt axis [2]

In addition, test 2 also exists for the forward stability of the counterbalanced trucks. The difference in this test compared to test 1 is that the payload is positioned at carry height (fork heel being 0.5 m above the ground) and the mast is fully back tilted. The truck position on the tilt table is same as that of test 1 for test 2. After positioning the truck as shown in Figure 2.3a, again the angle $\alpha_{st\_\text{threshold}}$ is noted.

Test 3/4: Lateral Stability

This test is conducted to evaluate the lateral stability of the truck. The truck is positioned in a turned position such that the roll axis MN of the truck is parallel to the tilt axis XY shown in Figure 2.5. The rated load is placed at the load center with the mast fully back tilted and raised to maximum height, as shown in Figure 2.3b. After meeting all position requirements, the platform is rotated about the XY axis until the front outer wheel has lifted off the ground. The tilt angle at which the front outer tire looses contact from the ground is noted. For safety, the truck is constrained with help of ropes so that it does not roll over completely.

Furthermore, test 4 exists comprising of two parts: test 4 Wheel Lift (WL) and test 4 Ultimate (ULT) which also evaluate the lateral stability of the lift truck. In this test, the mast is fully back-tilted with the payload eliminated from the mast and rest all the conditions remain same as were in test 3. For test 4 WL, the front outer wheel of the truck is monitored and the test ends when the wheel leaves the ground surface. However, for test 4 ULT, the rear outer wheel is monitored. The test is terminated when the truck reaches a situation where it completely rolls over. In each test, the platform tilt angle values are observed when the respective wheel of the truck has no contact with the ground anymore. As mentioned, ISO has set minimum slope requirements which a truck must meet. Moreover, the Hyster forklift H9XD6 claims to be more stable and has greater stability limits. The respective ISO minimum requirements and the truck's actual stability limits are presented in Table 2.1.

Table 2.1: ISO 22915: verification of stability - minimum requirements [2]

Stability Test	**ISO min req. slope [%]**	**Stability limit [%]**
Test 1 (Forward rated load raised)	3.80	6.08
Test 2 (Forward rated load lowered)	18.00	24.97
Test 3 (Lateral rated load raised)	6.30	11.35
Test 4 WL	No std.	49.18
Test 4 ULT	50.00	91.53

2.3 Multibody modeling

Multibody modeling has been an important asset to contribute towards developing virtual tools to solve problems that are too difficult to capture using analytical models. Alberto Martini presented a study in which he created a virtual testing tool based on the multibody model to evaluate dynamic stresses experienced by a forklift [6]. Another research conducted by Marco Pinelli shows a multibody model of a forklift being used to predict dynamic loads on the truck [7]. Similarly, developing a multibody model to simulate dangerous scenarios can solve the current knowledge gap in identifying unstable situations encountered by a forklift in dynamic conditions.

To develop the required model, apart from the literature from Alberto [6] and Pinelli [7], the lecture on multibody dynamics by Nathan Van De Wouw [8], is used. Following the approach of Nathan, a schematic diagram of the forklift truck is formulated comprising different rigid bodies representing truck components connected by joints. A previous study on multibody modeling is summarised that has similar details to the model described in this research. This study presents a developed and validated multibody model of Renault Twizy [9] which is divided into subsystems such as chassis, drive train, drive axle and steer axle. The assumption made is that the bodies modeled have mass and volume but are infinitely stiff. Modeling rigid bodies improves solving time and makes the differential equations simpler [10]. To model contact with the road surface, Baaij used the TNO Delft tire model, which treats the tire as a single rigid disc and is validated using measurements of a rolling tire between 7 and 40 m/s [11]. The Magic Formula (MF) tire force and torque block, available in Simscape, is based on the same concepts as of the TNO Delft tire model and is used in this thesis. The multibody models developed in [9],[12] and [13] were validated by conducting static and dynamic tests. Researchers conducted static tests which comprised of accessing the center of gravity and mass distribution of the developed vehicle model and the dynamic tests concentrated on determining the steady state and dynamic behavior of the developed model. This process of model validation helps in an overall assessment of the model quality. Instead of estimating the model quality visually, correlation coefficients such as Pearson's correlation coefficient (R) is calculated in the research of Jan Loof [14] to quantify model results. In addition, it is concluded that the Pearson's correlation coefficient alone is not enough while comparing model results with measurements as it does not take into consideration the offset which might be present between the two compared signals. Therefore, an offset error (ϵ) and Normalised Root Mean Square Deviation (NRMSD) are also calculated in the research conducted by Backhuijs [13]. With the help of the listed correlation coefficients, Backhuijs developed an accuracy criterion. A similar approach is also followed in this master thesis as this has been done in the past and has provided reliable agreement between measurements and model results.

2.4 Identifying critical instability scenarios

After validating the multibody model, critical scenarios are modeled to observe the behavior of the truck and detect instabilities. Scenarios under which the truck reaches the threshold lateral/longitudinal accelerations calculated by (2.1) and (2.2) are taken into consideration. Research conducted by Larsson [15] highlights some of the fatal incidents caused by forklift trucks where the truck can develop high lateral/longitudinal accelerations. The critical scenarios comprising of sudden braking/accelerating and cornering events are modeled based on the above study.

After simulating the critical scenarios, a visual and mathematical analysis of the truck's behavior is conducted. The effect of maximum acceleration, deceleration and cornering on the truck can be observed with the help of several metrics, such as the Lateral Load Transfer Rate (LLTR), roll rate of the truck and CoG position, as studied in [16], [17] and [18]. CoG position is considered one such metric to indicate stability as rollovers are caused typically by the high position of the CoG of a vehicle mentioned in the research conducted by Yunbo Hou [16]. Also, in static and steady-state situations, the concept of stability triangle, explained in Section 2.1, can be used to identify unstable situations. Moreover, the second metric used to predict roll over in Yunbo's research is the Rollover Index (RI) which is also called the Lateral Load Transfer Rate in [17] and [18]. The risk of roll over increases when the RI exceeds 0.8 for any prolonged period. This is an important indication and is therefore considered a metric to identify unstable situations. Since RI indicates lateral stability, based on the concept of RI, a stability metric for indicating forward stability is also developed in this thesis.

Based on the metrics mentioned above, boundary conditions comprising of critical velocity and lateral/longitudinal accelerations are created. For example, in a critical scenario of a high-speed corner, the RI, is monitored. The instant where the RI crosses 0.8, it is known that the truck is approaching a rollover and indicates danger [17]. At the point of criticality, values of parameters such as lateral acceleration and velocity can be noted. These are the critical values of the mentioned parameters above which a truck approaches instability. This data holds the potential for the development of an alert system, which in turn can be used to aware the driver of an approaching danger.

2.5 Summary

The first section of this chapter gives insight into the stability concepts of a forklift. It is concluded that depending on the location of the combined CoG (forklift and payload), stability can be approximated for static situations. If the CoG of the truck lies within the stability triangle, the truck is said to be stable. Whereas for steady state conditions, it is the resultant force acting on the CoG which should meet the ground surface inside the stability triangle to make sure that the truck is stable. Subsequently, the ISO 22915 verification of stability tests are explained which account for forward and lateral stability of a counterbalanced truck. ISO has determined minimum standards which a truck must satisfy to prove that the truck is safe to be operated commercially. These values depict the minimum slope at which all the resultant forces acting on the CoG of the truck should meet inside the stability triangle boundary. This denotes, the truck should be stable at the slope values provided by ISO.

Previous studies related to multibody modeling are discussed which have helped in developing a systematic model approach for this thesis. Also, tests conducted to validate several multibody models along with several correlation coefficients to quantify the model results are also presented. Lastly, metrics such as RI and location of CoG are discussed which are used in this thesis to identify critical instability scenarios and formulate boundary conditions.

Chapter 3

Dynamics of a rear-wheel steered vehicle

The forklift analyzed in this thesis is the Hyster H9XD6, which, like its counterparts, employs a rear-wheel steering configuration. Since the forklift is equipped with the front end assembly comprising of mast, carriage and forks, a rear wheel steering configuration is favoured due to space constraints. Most importantly, rear wheel steering configuration offers to follow a tighter turning radius which allows the forklift trucks to operate in narrow aisles [19]. Therefore, the majority of forklifts are equipped with a rear-wheel steering mechanism.

However, there is a difference between a front and a rear-wheel steered vehicle in the way in which a turn is initiated. For a front-wheel steered vehicle, the front wheels steer in the same direction as the desired turn, resulting in generating lateral forces towards the instantaneous center of rotation immediately. Whereas, in a rear-wheel steered vehicle, the rear tires steer in the opposite direction of the desired turn. This raises several questions related to the behavior and direction of the lateral forces that arise when steering the rear tires. Hence, the bicycle model is used to investigate the behavior of lateral forces and accelerations for vehicles equipped with rear-wheel steering only.

The bicycle model is a single track vehicle model in which the left and right tires are lumped into a single tire along the center line of the vehicle. Along with the main assumption of lumping the tires and axle characteristics into an equivalent tire, center point steering is assumed with no body roll. There are two degrees of freedom for the CoG in a single track vehicle model which are the lateral velocity (v) and yaw velocity (r). This model is developed to study the impact of a steering angle (δ) on the yaw dynamics of the vehicle. The concept of instantaneous center of rotation is an important concept when it comes to vehicle turning which is explained in the following section.

3.1 Instantaneous center of rotation

The Instantaneous Center (IC) of rotation, also known as the Instantaneous Center of zero velocity, is an imaginary point in the plane of motion at which the instantaneous velocity is zero and the rigid body rotates about that point. For a front-wheel steered vehicle, considering that the rear tire does not develop a side slip angle, the IC is located on an imaginary line formed by extending the rear axle. On the other hand, the rear wheels do form a small side slip angle due to sliding, therefore, the IC shifts forward to maintain a right angle with the velocity vector of the tire [20],[21]. Figure 3.1 shows top view of the single track vehicle

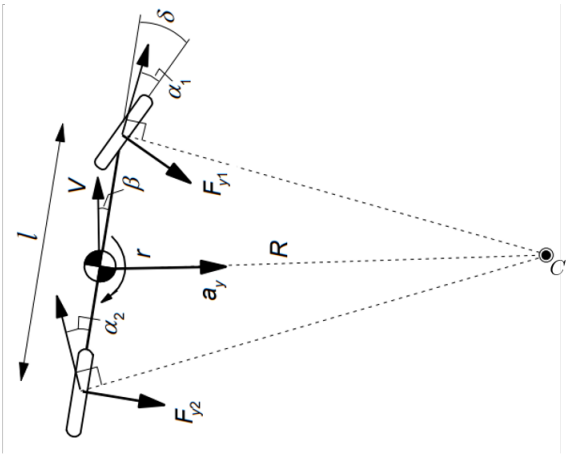

Figure 3.1: Steady state cornering: single track vehicle model [21]

model in a steady state cornering situation. The vehicle is rotating about the IC denoted by C in Figure 3.1. The vehicle is steered by the front wheel giving a steering angle (δ). Hence, the velocity vector is not along the plane of symmetry for the front and rear tires giving rise to side slip angles denoted by α_1 and α_2 in Figure 3.1. With the side slip angles developed, the lateral forces on the front and rear tires are perpendicular to the wheel of symmetry.

Figure 3.2 depicts the steady state turning condition for a rear-wheel steered vehicle. The IC is located on the imaginary line formed by extending the front axle considering no side slip angle is developed by the front wheel as shown by point C in Figure 3.2. However, as mentioned, non-steered wheels also develop small side slip angles. Therefore, it is concluded that the location of IC has to be ahead of the front axle denoted by point C' in Figure 3.2 when the front and rear tires develop side slip angles. This is necessary as the velocity vector at the tire has to be at right angle with respect to the turning radius. Only then, it is possible to have both lateral forces pointing towards the IC which makes evident that the vehicle follows the path of the desired turn.

From the explanation of Figure 3.2, it is concluded that in order to make a steady-state turn for a vehicle, both lateral forces should point in the direction of the desired turn, which is irrespective of a front-wheel or a rear-wheel steering configuration. In order to obtain such a condition, the instantaneous center of rotation moves ahead of the front axle for a rear-wheel steered vehicle.

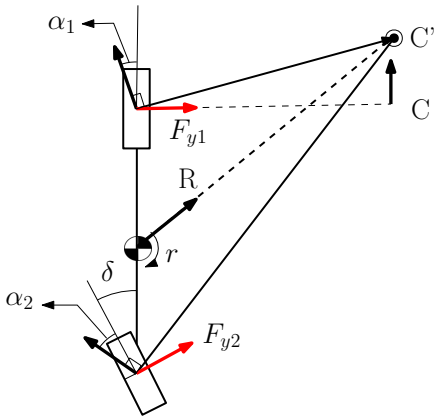

Figure 3.2: Rear wheel steered vehicle: location of IC

3.2 Dual steer bicycle model

To study the dynamic behavior and observe the yaw dynamics of a rear-wheel steered vehicle, a dual steer bicycle model is developed. The equations of motion for the bicycle model as studied from the vehicle dynamics lecture notes [21] are shown below:

$$m(\dot{v} + ur) = F_{y1} + F_{y2}, \tag{3.1}$$

$$I_{zz}\dot{r} = aF_{y1} - bF_{y2}, \tag{3.2}$$

where m is the mass of the vehicle, I_{zz} is the yaw moment of inertia, v is the lateral velocity, u is the forward velocity and r is the yaw velocity of the vehicle. The longitudinal distance to the CoG of the vehicle from the front and rear tire is given by a and b, respectively. The lateral tire forces are only considered in the linear range for small side slip angles shown by the following expression:

$$F_{y1} = C_1 \cdot \alpha_1, \tag{3.3}$$

$$F_{y2} = C_2 \cdot \alpha_2, \tag{3.4}$$

where C_1 and C_2 are the cornering stiffnesses for the front and rear tires, respectively. As shown in Figure 3.3, for a dual steer bicycle model, the expressions of side slip angles α_1 and α_2 are crucial which have the effect of the front and rear steering angles, δ_1 and δ_2 respectively. The expression for the side slip angles as studied from [22] are given below:

$$\alpha_1 = \delta_1 - \frac{(v + ar)}{u} \tag{3.5}$$

$$\alpha_2 = \delta_2 - \frac{(v - br)}{u} \tag{3.6}$$

By substituting (3.3) to (3.6) in the two equations of motion (3.1) and (3.2), two detailed equations are obtained for a dual steer bicycle model presented below:

$$m\dot{v} + \frac{1}{u}(C_1 + C_2)v + r(mu + \frac{1}{u}(C_1a - C_2b)) = C_1\delta_1 + C_2\delta_2 \tag{3.7}$$

$$I_{zz}\dot{r} + \frac{1}{u}(aC_1 - bC_2)v + \frac{1}{u}(a^2C_1 + b^2C_2)r = aC_1\delta_1 - bC_2\delta_2 \tag{3.8}$$

The two equations are put in a state space form to analyze the dynamic behavior.

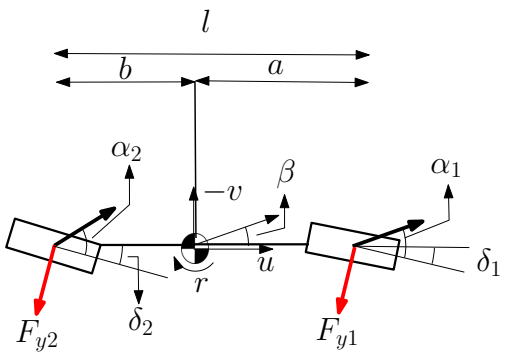

Figure 3.3: Dual steer bicycle model [22]

State-space representation

The dynamic behavior of a rear-wheel steered bicycle model is analyzed by a state space representation of (3.7) and (3.8). The dynamics are represented by state space matrices whose general form is:

$$\dot{x} = Ax + Bu,$$
$$y = Cx + Du,$$

where x being the state vector, u the input vector, y the output vector and A,B,C and D are the matrices formed by (3.7) and (3.8).

The lateral velocity and yaw velocity are used as the states and the steering angles are provided as input to the state space model. The output consists of the lateral acceleration, yaw rate and the vehicle side slip angle as shown below:

$$x = \begin{bmatrix} v \\ r \end{bmatrix}, u = \begin{bmatrix} \delta_1 \\ \delta_2 \end{bmatrix}, y = \begin{bmatrix} a_y \\ r \\ \beta \end{bmatrix} = \begin{bmatrix} \dot{v} + ur \\ r \\ -\frac{v}{u} \end{bmatrix}$$

The A,B,C and D matrices for a dual steer bicycle model are given by:

$$A = -\begin{bmatrix} \frac{C_1+C_2}{mu} & u + \frac{aC_1-bC_2}{mu} \\ \frac{aC_1-bC_2}{I_{zz}u} & \frac{a^2C_1+b^2C_2}{I_{zz}u} \end{bmatrix}, B = \begin{bmatrix} \frac{C_1}{m} & \frac{C_2}{m} \\ \frac{aC_1}{I_{zz}} & -\frac{bC_2}{I_{zz}} \end{bmatrix}$$
$$C = -\begin{bmatrix} \frac{C_1+C_2}{mu} & \frac{aC_1-bC_2}{mu} \\ 0 & -1 \\ \frac{1}{u} & 0, \end{bmatrix}, D = \begin{bmatrix} \frac{C1}{m} & \frac{C2}{m} \\ 0 & 0 \\ 0 & 0 \end{bmatrix}$$

In order to represent the the dual steer bicycle model as only a rear-wheel steered bicycle model, the front steering angle (δ_1) is assumed to be 0. The state space representation is replicated in MATLAB and time response of the dynamic system is simulated using the command '*lsim*' by giving a step input of -1 deg. rear wheel steering angle (δ_2). The following parameters of the forklift truck are used during the simulation: $m = 14632$ kg, $I_{zz} = 94680$ kgm^2, $l = 2.7$ m, $a = 1.225$ m, $C_1 = C_2 = 60000$ N/rad. The step steering input provided to the rear wheel is shown in Figure 3.4.

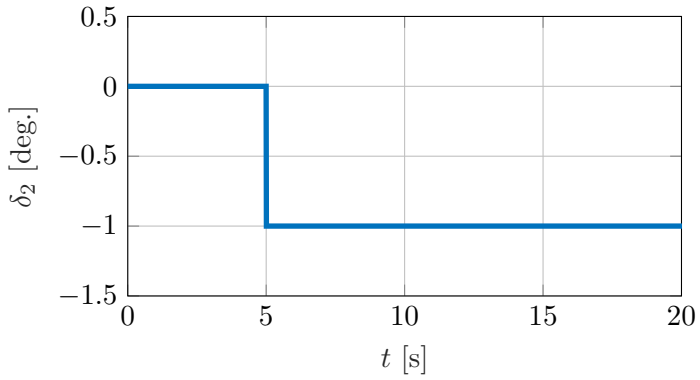

Figure 3.4: Rear wheel step steering input

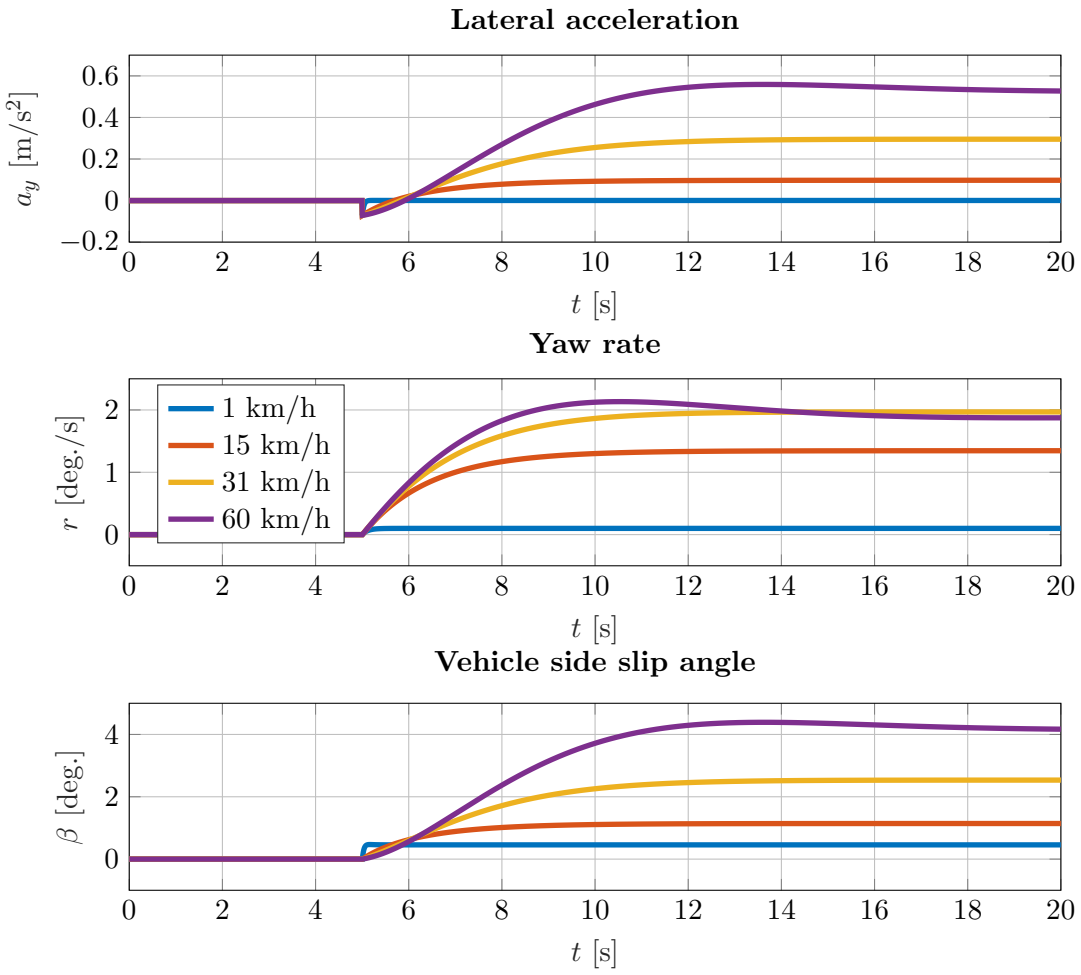

Figure 3.5: Step response: −1 deg. rear steering angle (δ_2)

Figure 3.5 illustrates the yaw rate, vehicle side slip angle, and lateral acceleration with respect to time (t) for increasing forward velocities. The yaw rate plot depicts that the yaw rate gradually stabilizes without an overshoot for smaller velocities. For higher velocities, the yaw rate stabilizes after a slight overshoot, similar to typical front-steer vehicles.

The vehicle side slip angle (β) can be related to the front side slip angle (α_1) as shown:

$$\alpha_1 = \delta_1 - (\frac{v + ar}{u}) = \delta_1 - \frac{v}{u} - \frac{ar}{u}$$

For a rear-wheel steered vehicle, $\delta_1 = 0$ and considering circular driving with fixed radius R ($rR = u$):

$$\alpha_1 = \beta - \frac{a}{R} \tag{3.9}$$

$$\beta = \alpha_1 + \frac{a}{R} \tag{3.10}$$

For a front wheel steered vehicle, the side slip angle changes sign as the vehicle velocity is increased [21], however, the vehicle side slip angle in the case of a rear wheel steered vehicle

always remains positive, evidently shown by (3.10) and Figure 3.5.

The lateral acceleration also exhibits a unique behavior in a rear wheel steered vehicle. The time instant when a step steer input is provided to the rear wheel, as an initial tire response, the tire produces a lateral force in the opposite direction. The lateral force produced in the opposite direction results in a negative lateral acceleration step, seen in Figure 3.5. Subsequently, the lateral force builds up in the correct direction to keep the vehicle on the path following the desired turn. This also results in a sign change of the lateral acceleration, evidently shown in Figure 3.5.

3.3 Summary

This chapter discussed the dynamics of a rear-wheel-steered vehicle, revealing significant disparities in comparison to front-wheel-steered counterparts. The vehicle dynamics were examined through the implementation of a dual-steering, bicycle model. Initially, the instantaneous center of rotation for a rear-wheel-steered vehicle was determined. It was concluded that, in this case, the IC is positioned beyond the front axle, resulting in generating the lateral forces in the appropriate direction of turning.

Furthermore, the dynamic response of a rear-wheel steered vehicle was then investigated using a state space representation of the bicycle model incorporating forklift parameters. Notably, the yaw rate follows similar behavior to the standard front-wheel steered vehicle. However, distinctive behavior emerged when considering the vehicle side slip angle and lateral acceleration. Unlike the front-wheel steered vehicle, the vehicle side slip angle remains consistently positive under both low and high accelerations. On the other hand, initially the lateral acceleration starts in the opposite direction of the turn due to a step input applied on the rear wheels. Afterwards, the lateral acceleration switches signs.

Chapter 4

Multibody Forklift Model

A multibody forklift model is developed to identify critical instability scenarios. This chapter explains the modeling of the Hyster H9XD6, being the subject of investigation for this study. The model development approach is formed by utilizing the multibody modeling concepts discussed in Section 2.3.

4.1 Model overview

The lift truck model is developed in MATLAB/Simulink using the Simscape Multibody toolbox. This toolbox enables to model components as separate bodies, which are connected with the help of joints. Subsystems that are defined mathematically such as the brakes and the powertrain are modeled using Simulink and connected to multibody components using converter blocks available in Simulink.

The coordinate system used to develop the model is defined according to the international norm ISO 8855 [23] shown in Figure 4.1. The x axis is oriented in the forward direction of driving and the z axis is oriented perpendicular to the road surface pointing upwards as shown in Figure 4.1b. The y axis is perpendicular to the x and z axis, as shown in Figure 4.1a. It is preferred to use the ISO sign conventions as it is widely used in the industry and the subsystems available in MATLAB are also formulated using ISO 8855. The ground level is assumed at $z = 0$ and the origin of the vehicle coordinate system is situated at the center of the front axle projected on the ground. This choice is made as the data available provides information about the dimensions and inertial properties of components with respect to the front axle of the vehicle.

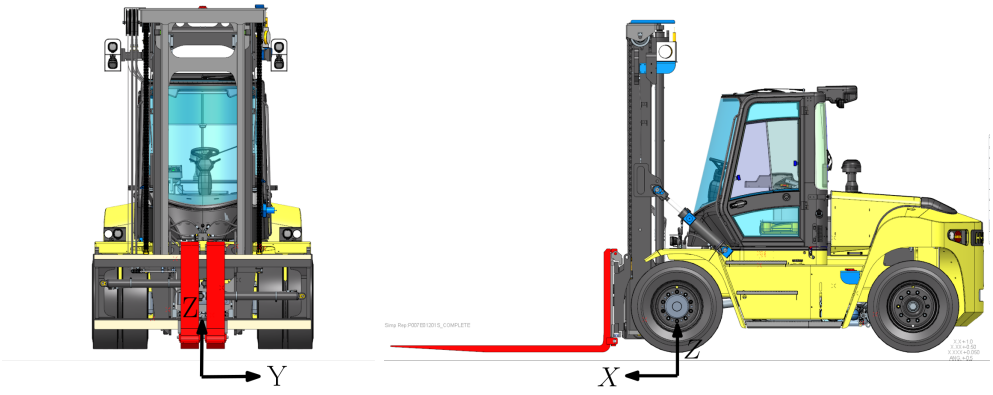

(a) Front View **(b)** Side View

Figure 4.1: ISO 8855 Coordinate system

As a part of the model development, a schematic diagram is prepared to get an overview of the vehicle model. The model is divided into subsystems such as chassis, drive axle, steer axle, front-end equipment, powertrain and braking. One of the unique subsystems in this model is the front-end of the truck comprising of mast, carriage and forks. The schematic diagram, shown in Figure 4.2, summarises the interaction between components. As can be seen in Figure 4.2, the forklift model is simplified as compared to reality and seen from a multibody point of view. For example, the lift cylinders in the forklift are used for lifting and lowering the mast, whereas in the model, instead of using actual cylinders, a prismatic joint that allows translational motion is used. The tires are connected to the respective axles with a revolute joint, which allows the wheels to rotate along one axis. For the steer axle, tires are equipped with two revolute joints, one for rolling and the other for steering. To represent a rigid connection between two bodies, a weld joint is used in the model. The powertrain and braking subsystem are modeled using a Simulink block diagram. The summarised model simplification has helped in attaining the research goal of predicting the stability of the lift truck with less challenges and also reducing complexity and computation time simultaneously.

The model is used to simulate several critical scenarios given a set of vehicle parameters and driver inputs. This is fulfilled by creating a MATLAB script which functions in three stages. First, all the vehicle parameters and inputs necessary to define the vehicle and tests conditions are loaded. The vehicle parameters consist of the dimensions and inertia properties of the components modeled. Inputs to the model are velocity or throttle pedal position, brake pedal position, steering angle, lift height and mast inclination angle. After loading the parameters and prescribing inputs, the model is simulated in Simulink and a separate window for a visual representation of the simulation is opened. This makes it easy for the user to comprehend the given inputs to the model and observe the behavior of the system. After the simulation, post-processing of the simulation output is carried out where correlation coefficients are calculated and graphs can be generated. In addition, stability metrics are calculated to identify the time instant where the truck is close to rolling or tipping over. Appendix A gives an explanation of the structure and operation of the forklift multibody model in detail.

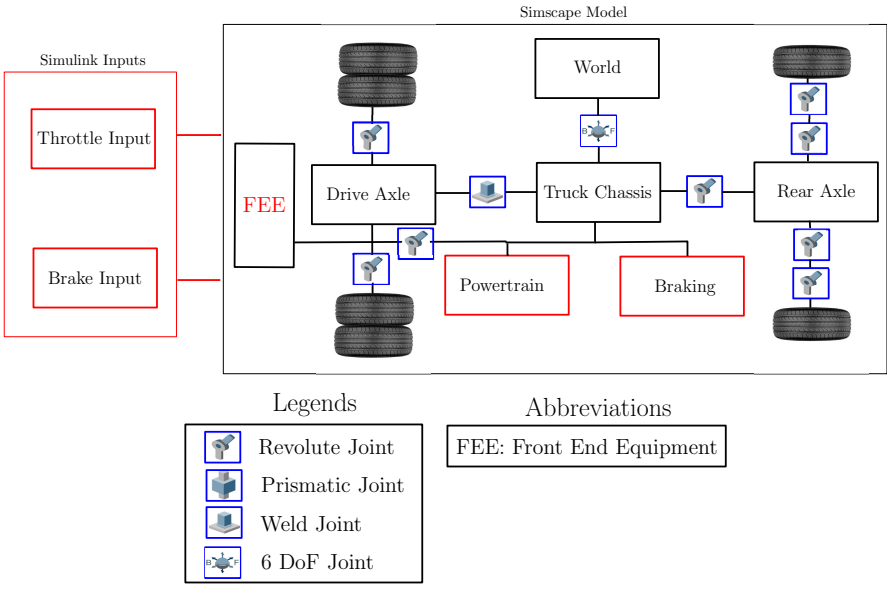

Figure 4.2: Forklift multibody model: schematic representation

4.2 Model implementation

Following the model development approach explained in Section 4.1, the implementation of each subsystem is discussed in this section. While developing the multibody model, data has been used from CAD software and various design specification documents. The data gathered provide information on the mass, inertial properties and CoG coordinates of the components defined with respect to the front axle of the forklift. Information regarding component dimensions is used to calculate respective distances for connection points between different components.

4.2.1 Chassis

The chassis subsystem is graphically represented by a solid body in Simscape with dimensions approximated close to reality for visual representation. CoG coordinates are defined using the local axis system of the body. The mass and moments of inertia are available from the data gathered by design-specific documents and applied at the CoG of the chassis. A 6 Degree of Freedom (DoF) joint is used to connect the chassis to the world frame, which allows the chassis to move freely in space. Since the 6 DoF joint allows free movement of the chassis, the vehicle behavior in cornering and braking situations giving rise to lateral and longitudinal load transfer can be observed.

4.2.2 Drive and steer axle

Two additional frames are defined on the front and back side of the chassis to link the drive and steer axle, respectively. The drive axle is rigidly connected to the truck frame without any suspension mechanism, therefore, a rigid connection is established between the chassis and the drive axle with the help of a weld joint. The two ends of the front axle are connected to the tires with the help of revolute joints to allow rolling/braking of the front tires. These revolute joints are actuated by providing the combined torque from the powertrain and braking subsystem.

The rear axle does not have a rigid connection with the chassis and is connected with the help of a pivoting tube with the chassis. With this, the steer axle can pivot along the x axis of the vehicle as shown in Figure 4.3a ranging from -8 to 8 degrees. This is done to minimize the torsion forces on the chassis when the truck is driving on an uneven surface. After reaching the limits of ± 8 degrees, the rear axle comes in contact with the truck chassis acting as a hard stop to this pivoting motion.

In Simscape, this pivoting motion of the rear axle is established with the help of a revolute joint that can rotate along its fixed z axis. To achieve the pivoting motion of the steer axle along the x axis of the vehicle, a frame transformation is performed using the rigid transform block in Simscape. To model the contact between the rear axle and the chassis at the limits, the revolute joint is actuated by a torque (T_{pivot}) with respect to the pivot angle (θ_{pivot}) of the rear axle shown in Figure 4.3b. The revolute joint has no torque actuation between -8 to $+8$ degrees and is free to rotate, as seen in Figure 4.3b. However, once these limits are reached, the revolute joint applies a torque in the opposite direction to stop the revolute joint from rotating. A linear stiffness of 11500 Nm/deg. is introduced after exceeding ± 8 degrees of rotation as shown in Figure 4.3b. Along with the stiffness, the revolute joint also has a damping coefficient of 10 Nms/deg to avoid sudden contact of the rear axle with the chassis. This way the rotation of the revolute joint is restricted to ± 8 degrees.

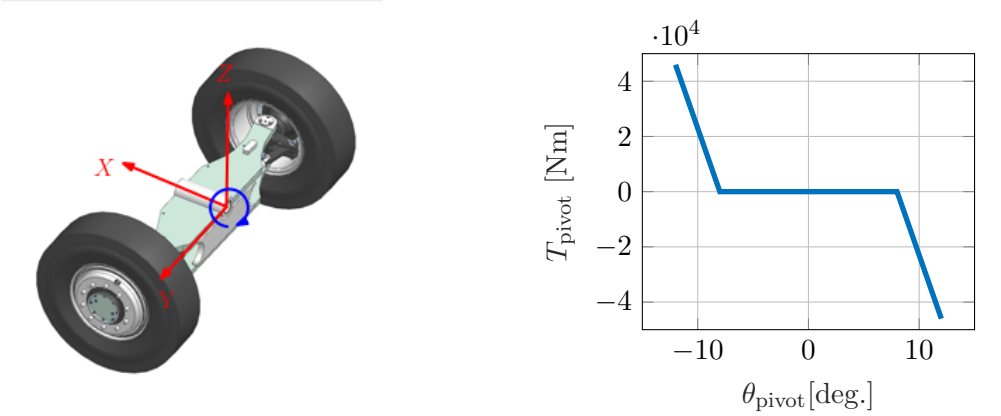

(a) Pivoting tube **(b)** Actuator torque for pivoting motion

Figure 4.3: Rear axle connection to truck chassis

The two ends of the rear axle are further connected to the tires with the help of revolute joints. Since the forklift is rear wheel steered, there is a revolute joint per side allowing the tires to rotate along the z axis for steering. Furthermore, there also exist a revolute joint per side allowing the tires to rotate along the y axis to roll, similar to the front axle.

4.2.3 Tires

The Hyster forklift H9XD6 is equipped with Trelleborg Elite XP 10.00 - 20.00/8.00 solid tires on both the drive and steer axle. The drive axle of the lift truck has dual front wheels, meaning there are two tires per side on the front axle as shown in Figure 4.1a. Since lift trucks carry a high fraction of load on the front axle, the front axle equipped with four tires helps to keep the load per tire within reasonable limits. Therefore, six tires in total are modeled in Simscape with different approaches depending on specific use cases. For dynamic driving, the Magic Formula (MF) tire force and torque block is used. Whereas, to simulate the ISO 22915: verification of stability tests two approaches are developed as the MF tire force and torque block cannot be used directly. The mentioned approaches are explained in subsections 4.2.3.1 and 4.2.3.2.

4.2.3.1 Dynamic tire modeling

The MF tire force and torque block implements the combined slip steady state Magic Formula for a rolling tire. The block calculates the slip forces and torques for the tire; therefore, inertia properties of the tire including the rims are specified using a cylindrical solid block. The implementation of this tire block is straightforward with certain user-specified inputs: tire side, tire parameters and slip mode. The tire side is specified for each tire depending on left or right and the combined slip mode is used.

To specify tire characteristics, a tire property file with the extension .tir is required which contains the Magic Formula parameters. Since the truck is equipped with solid tires for which the tire property file is not available, .tir file of a Bridgestone 315/80 R22.5 pneumatic tire of a commercial vehicle is altered and used. The tire property file used for simulations does not match with real tires and might cause deviations in model simulations.

Since the tire model described above, is only applicable to rolling tires, a different approach to model the non-rolling tire contact on an inclined surface is necessary. Non-rolling tire modeling is crucial for this research as the multibody model is used to simulate the ISO 22915 stability platform tests discussed in Section 2.2. The dynamic MF tire model can be used to simulate the stability platform tests in which the truck has to remain stationary on an inclined surface at the cost of increasing the simulation time. The lower boundary velocity in slip calculation, known as $V_{x,\mathrm{Low}}$ in the (.tir) file, is normally specified to be 1 m/s. If the value for $V_{x,\mathrm{Low}}$ is decreased, then the tires can function for these static stability tests without sliding on an inclined surface, but the computation time increases considerably. Therefore, two different approaches for efficient modeling of non-rolling tire contact on an inclined surface are developed.

4.2.3.2 Non-rolling tire modeling

There are two approaches through which the contact between the truck body and the road surface is modeled in this thesis. These are explained below:

Tire as a bushing joint

The first approach involves bushing joints to represent a non-rolling tire in Simscape. Figure 4.4 represents a schematic diagram, which shows a bushing joint representing contact between the axle and the ground surface. A bushing joint has two frames known as the base and follower frame, through which it can be connected to different bodies in Simscape. The base frame of the bushing joint is connected to the truck axle and the follower frame is connected to the ground surface as shown in Figure 4.4.

The bushing joint in Simscape also has the possibility to provide three translational and three rotational degrees of freedom along with providing stiffnesses in all three directions. By providing the longitudinal, and lateral stiffnesses in the x and y directions, respectively, the stiffness characteristics of a tire are modeled. Furthermore, the linear vertical stiffness of the tire is modeled by an actuator force considering the tire as a combination of spring and damper given by the following expression:

$$F = K_z \cdot x + b_{\mathrm{damp}} \cdot \dot{x}, \tag{4.1}$$

where F is the actuator force, K_z is the vertical stiffness of the tire, x is the tire deflection, $\dot{x}$ is the relative velocity at the tire contact patch and b_{damp} is the damping coefficient.

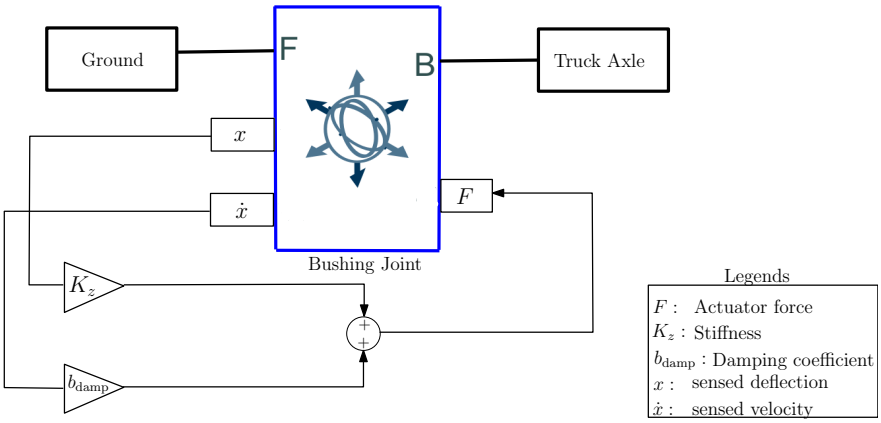

Figure 4.4: Non-rolling tire modeling: approach 1 using bushing joint

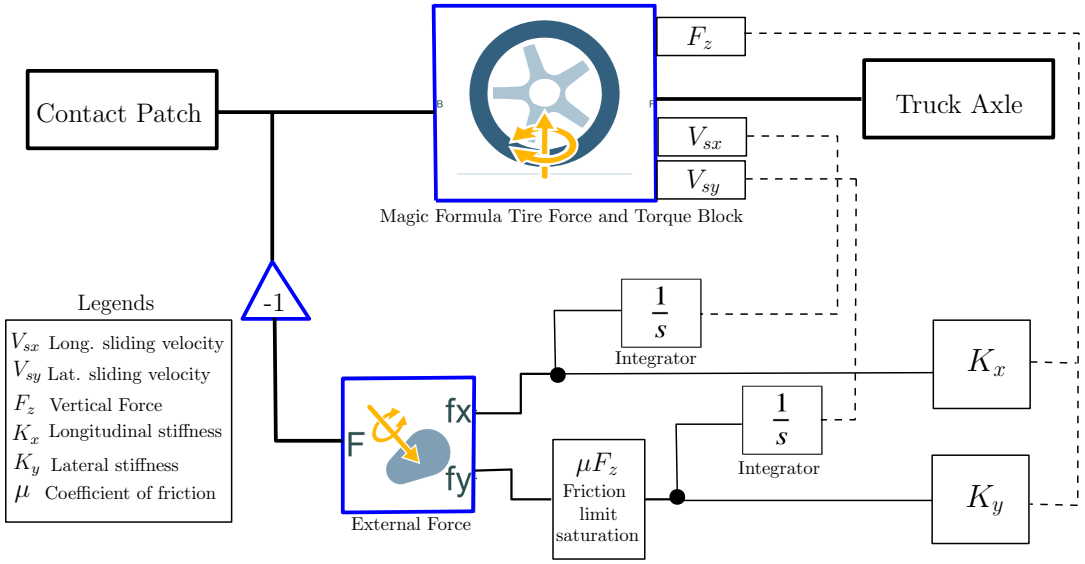

Figure 4.5: Non-rolling tire modeling: approach 2 using MF tire block

The available data between the applied load and measured deflection of the actual equipped tire is used to formulate a look up table. This look up table is used to calculate the normal force on tire with respect to the deflection measured and the vertical stiffness (K_z) of the tire is determined. As shown in Figure 4.4, the product of vertical stiffness and the sensed tire deflection is used to calculate the spring force. The sensed velocity and the damping coefficient equal to 1500 Ns/m (as used for dynamic tire model) is used to calculate the damping force. Further, the addition of the two calculated forces results in an actuator force. With this implemented, if the tire loses contact with the ground, there will be no deflection and velocity at the contact point. Hence the vertical stiffness of the tire will also not exist.

Approach 1 using the bushing joint is a fair representation of a tire. However, the user involvement in this approach is considerable leading to high chances of mistakes. Therefore, initial steps are taken to develop a more straight forward and efficient approach using the MF tire force and torque block.

Modified Magic Formula tire force and torque block

The second approach involves the MF tire force and torque block, but with slight alterations to represent the tire in an inclined static condition. When the tire is placed on an inclined surface, it starts to slide if the $V_{x,\text{Low}}$ parameter is not reduced. On the other hand, reducing $V_{x,\text{Low}}$ does prevent the tire from sliding, but is directly proportional to increasing computation time. Therefore, a method is proposed which prevents the tire from sliding without reducing the $V_{x,\text{Low}}$. Figure 4.5 shows a schematic representation of the model developed to calculate an external force applied in the opposite direction of sliding to constrain the truck in the same position. As seen in Figure 4.5, both, the longitudinal sliding velocity (V_{sx}) and lateral sliding velocity (V_{sy}) are integrated to obtain displacements at the tire contact patch in the longitudinal and lateral directions. The longitudinal and lateral stiffness represented by (K_x) and (K_y), are calculated with the help of a look-up table providing vertical force as input. Thereafter, using the respective displacements along with the respective stiffnesses, the magnitude of the forces acting in the x and y directions are determined. The lateral force obtained in the y direction is saturated depending on the vertical force on the tire so that it does not exceed the friction limits of a tire. Finally the obtained forces at the tire

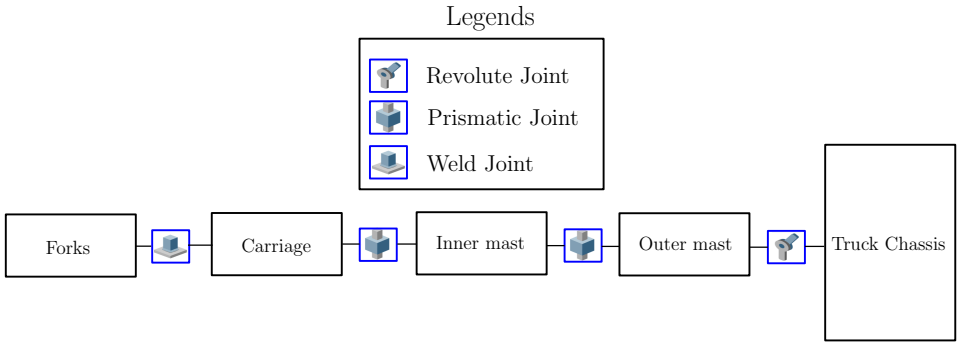

Figure 4.6: Front-end assembly: schematic representation

contact patch are applied in the opposite x and y directions to avoid tire sliding. This is done with the help of an external force block and a negative gain, as shown in Figure 4.5. This approach being more straight forward as compared to approach 1 is also used to simulate the ISO 22915: verification of stability tests.

4.2.4 Front end equipment

The front end assembly consists majorly of a mast, carriage and forks. The mast further consists of two components, namely, the outer mast which is connected to the chassis of the truck and the inner mast which is connected to the outer mast. The inner mast slides on the walls of the outer mast with the help of a roller-chain mechanism and lift cylinders to attain the desired height in reality. The carriage is connected to the inner mast also with the help of rollers and is used to link the forks with the inner mast. The displacement ratio between the outer mast, inner mast and the carriage is designed such that the carriage is displaced twice as much as the inner mast with respect to the outer mast.

The schematic diagram shown in Figure 4.6 describes how components of the front end are linked to each other in Simscape. All components are modeled as rigid bodies with dimensions approximated for visual representation. The outer mast is connected to the chassis with the help of a revolute joint allowing the outer mast to tilt in the forward and backward direction. The revolute joint is actuated by providing the tilt angle allowing the mast to tilt 15 deg. in the forward direction and 12 deg. in the backward direction. The connection between the outer and inner mast is established with a prismatic joint. Similarly, the carriage is also connected to the inner mast with a prismatic joint. The prismatic joints for the inner mast and carriage are actuated by providing the displacements as input in the form of look up tables. These look up tables are formulated such that they consider the displacement ratio of inner mast and carriage with respect to the outer mast. The input provided to actuate the prismatic joints is passed through a second order filter with a response time of 0.05 seconds. This filtration is done to avoid abrupt changes of the input signal. Furthermore, a weld joint is used to connect the forks with the carriage. The side shifting of the forks in not modeled.

4.2.5 Steering system

The Hyster forklift H9XD6 is a rear-wheel steered truck and is equipped with a hydraulic power steering system, mechanically connecting the steering wheel and steered tires. A hydraulic cylinder is situated in the middle of the rear axle and is connected to both wheels mechanically with the help of steering arms. The truck is equipped with Ackermann steering

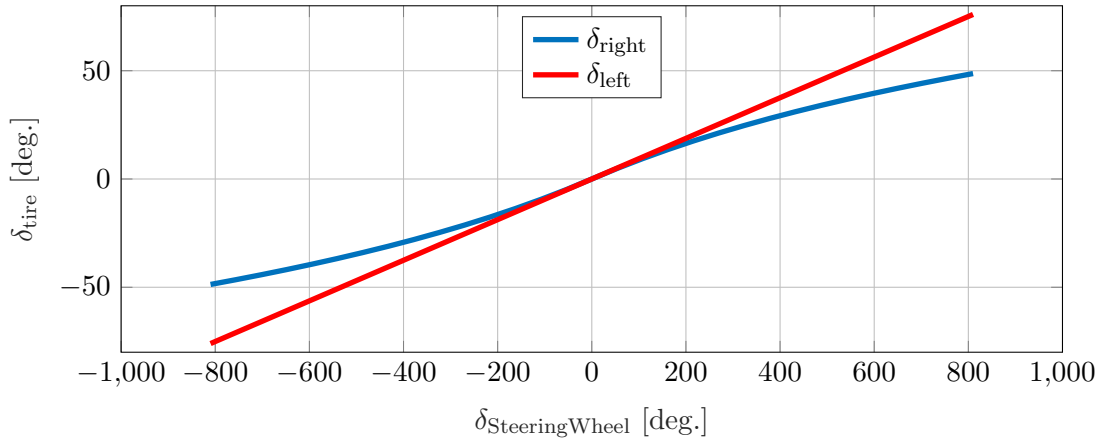

Figure 4.7: Steering geometry

geometry resulting in different left and right steering angles while turning. The inner tire has a greater steering angle as compared to the outer tire to avoid tire sliding and wear [24]. Generally, forklifts can develop large steering angles as the trucks are expected to function in narrow work spaces. The steering ratio is defined as the ratio between the steering wheel angle and the steering tire angle. Figure 4.7 shows the calculated Ackermann relation between the steering wheel angle and the steering tire angles used in the multibody model.

The steering system in the model is not modeled in detail, as the main aim of the research is to determine unstable situations of a forklift that do not depend on the steering geometry. The Ackermann steering geometry providing information about the left and right steering angles is used as a look up table in the model. The wheel hub is connected to the rear axle with a revolute joint which could rotate along the z axis to ensure steering of the tires. The revolute joint is actuated by providing a motion input representing the steering tire angle. The input provided to actuate the revolute joint is passed through a second order filter with a response time of 0.05 seconds to avoid abrupt changes in the input signal. Considering a left turn, the maximum angle allowed for the left and right steering tire is 76.00 deg. and 48.90 deg.,as can be seen in Figure 4.7. The steering angle input specified by the user is applied on the inner tire depending on the turn (left or right) and the outer angle is calculated by using the look up tables which use Ackermann steering geometry.

Alternatively, instead of providing the steering angle, the user can also provide the steering cylinder stroke which refers to the displacement of the steering cylinder piston when the wheels are turned. Data gathered from design specific documents provide relation between the steering cylinder displacement and the tire angles which is used in Simscape in the form of a look-up table.

4.2.6 Powertrain

Even though the project is related to analyzing the vehicle dynamics of the lift truck, a powertrain system is necessary to propel the driven wheels. A powertrain model is developed similar to an electric motor, which is a simplification of reality. The torque output of the powertrain is determined using the engine specifications and can be expressed as:

$$T_{\text{out}} = T_{\text{engine}} \cdot T_{\text{limitor}} \cdot \tau_{\text{throttle}}, \tag{4.2}$$

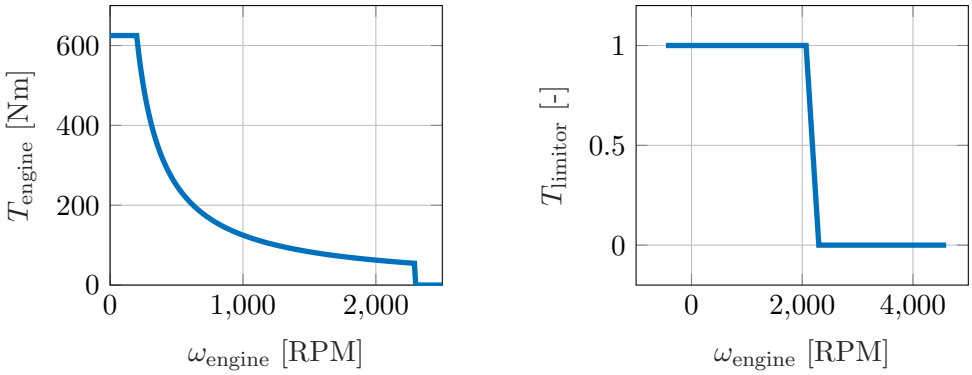

(a) Torque output **(b)** Torque limitor: $\text{RPM}_{\text{max}} = 2300$

Figure 4.8: Engine characteristics

where T_{out} is the output torque which is split equally between the driven wheels assuming an open differential with 100% efficiency. The obtained torque output is shown in Figure 4.8a. T_{limitor} is the rev limitor signal which decreases the output torque to zero after reaching the maximum engine RPM of 2300, as shown in Figure 4.8b. τ_{throttle} is the throttle pedal position which ranges between 0 and 1. The value of 1 denotes that the throttle pedal is fully actuated and 0 denotes no actuation. The throttle pedal position is an input from the driver model to the powertrain model where the drive torque is scaled with the help of this input. Furthermore, T_{engine} is the engine torque which is given by:

$$T_{\text{engine}} = \frac{P_{\text{engine}}}{\omega_{\text{wheel}} \cdot i_1 \cdot i_{fd}}, \tag{4.3}$$

where T_{engine} is the engine torque, P_{engine} is the available engine power, ω_{wheel} is the average of the angular velocity of both wheels, i_1 is the first gear ratio and i_{fd} is the final drive ratio. By this modeling technique, the torque output from the engine can be extremely high at angular velocities close to zero. Therefore, the engine torque is saturated based on the maximum torque the engine can deliver. Since only a single gear ratio is considered, the top speed is limited in this approach. Moreover, this powertrain is also used to simulate the lift tuck in reverse driving conditions as the truck has the same gear ratios for reverse driving. By providing a negative reference velocity, the output torque obtained from the powertrain is negative and the vehicle can drive in reverse direction.

4.2.7 Driver model

A driver model is necessary for the vehicle model as various input signals are required to conduct simulations. The driver model is responsible for providing inputs to the vehicle model such as the throttle pedal position and the brake pedal position, both scaled between 0 and 1. The multibody model also provides the possibility to use a cruise controller by providing a reference velocity profile with respect to time instead of throttle pedal position. Hence, the user can prescribe the following inputs through the driver module:

1. Vehicle velocity [km/h]
2. Throttle pedal position (scaled between 0 and 1) [-]
3. Brake pedal position (scaled between 0 and 1) [-]

Mostly, the model is simulated using the cruise controller by providing the velocity profile. The cruise control can also perform low deceleration, similar to engine braking. For high deceleration, the brake pedal position input is required. The implementation of the cruise controller and the braking system is explained next.

4.2.7.1 Cruise controller

The cruise controller used is similar to the cruise controller developed by Kempen [25]. The cruise controller used in this research compares the reference velocity provided by the user and the actual velocity of the vehicle measured by a transform sensor in Simscape. The difference between the reference velocity and actual velocity is the velocity error which is fed to a transfer function block which filters the error to avoid abrupt changes in the velocity. This filtered velocity error is then fed to a gain-based Proportional Integral (PI) controller which minimizes the error. The gains are available from previous research and are not tuned as the cruise controller functions well. The output of the PI controller is interpreted as the throttle position which is saturated between 0 and 1. The throttle pedal position is an input to the powertrain model where the drive torque is scaled depending on the throttle pedal position and the required torque on driving wheels is applied.

4.2.7.2 Braking

The lift truck is equipped with wet disc brakes on the front axle as service brakes. A parking brake functions when the truck is standing still on a slope. The rear axle is not braked and its wheels are left to roll freely.

The braking subsystem is simplified to achieve the required brake torque on the driving wheels. In the driver model, brake input is specified in terms of the brake pedal position. The brake pedal position must be between 0 and 1; 1 represents the pedal fully actuated and 0 represents that the pedal is not actuated. After the user specifies a brake input between 0 and 1 with respect to time, this input is passed on to the braking subsystem in the vehicle model. The maximum brake torque is calculated by the formula [21]:

$$M_{b,\max} = -(F_x)(r_t) = -\mu \cdot F_{z,\mathrm{FA}} \cdot r_t, \tag{4.4}$$

where $M_{b,\max}$ is the max. braking moment, μ is the coefficient of friction assumed to be 1 considering asphalt, $F_{z,\mathrm{FA}}$ is the vertical force on the front axle when standing still, F_x is the longitudinal force on tire and r_t is the tire radius. As mentioned, the brake input represents the brake pedal position scaled between 0 to 1 which when multiplied with the brake torque calculated by (4.4), represents the scaled brake torque to be split between the driven wheels. The brake torque is applied on the revolute joints connecting the front axle to the tires along with the drive torque produced by the powertrain. In the model, a linear relation between the pedal position and the magnitude of the brake torque is assumed for simplicity.

4.3 Summary

This chapter gave an insight into the multibody modeling of the Hyster forklift H9XD6. First, a model overview is provided which depicts the connection between different subsystems with each other. Section 4.2 discussed modeling aspects and implementation of each subsystem inside the forklift multibody model. In the next chapter, the developed model is validated by performing several static and dynamic tests.

Chapter 5

Model Simulation & Validation

This chapter discusses the steps taken to validate the multibody model of the Hyster forklift H9XD6. The validation process is divided into two categories; static and dynamic tests. The ISO 22915 verification of stability tests are also used as a means to validate the model. The data used to estimate the model accuracy in static situations is supplied by Hyster-Yale Group from the World Wide Rating Program (WWRP) used within the organization. The data gathered provide information about the mass distribution, CoG locations at different lift heights and ISO 22915 verification of stability tests results for the truck H9XD6. To validate the model response in dynamic situations, validation tests are conducted on the Hyster forklift H9XD6. These tests comprise of steady state circular driving and a test involving accelerations, cornering and braking.

5.1 Static validation

First, the truck is simply simulated standing still at two different fork heights which are: carry height (fork heel is 0.5 meters above the ground) and Maximum Lift Height (MLH) (fork heel is 4.675 meters above ground level). This simulation check provides information about the total truck mass, CoG of the complete truck and mass distribution on both axles. A lift truck can operate at carry heights going to approximately 5 meters above the ground. Hence, the CoG of the complete truck is affected and changes drastically during the lifting and lowering of the forks even when the truck is empty. The following data from the WWRP is taken to compare model results:

1. Truck mass
2. Mass distribution (front and rear)
3. CoG location at carry height
4. CoG location at MLH

The truck mass and CoG locations at different lift heights are extracted using an inertia sensor available in Simscape multibody toolbox. The base frame of the inertia sensor is connected to the world and the follower frame is connected to the origin of the model. Table 5.1 provides the comparison between the data gathered from WWRP and model results. The y CoG coordinate in the model is zero which denotes that the model is symmetric. Developing a symmetric model is preferred because, it makes easy to interpret results in dynamic situations involving lateral load transfer since the tires have equal vertical force on the left and right side.

Table 5.1: Comparison: Static mass and CoG coordinates

Parameters	WWRP	Model	Deviation [%]
Truck mass [kg]	14632	14632	0
Front mass [kg]	7990	8013	0.29
Rear mass [kg]	6642	6619	0.35
CoG at carry height [m]			
x - coordinate	-1.225	-1.221	0.33
y - coordinate	0.009	0	-
z - coordinate	1.072	1.080	0.74
CoG at MLH [m]			
x - coordinate	-1.225	-1.221	0.33
y - coordinate	0.009	0	-
z - coordinate	1.820	1.797	1.26

The last column of Table 5.1 denotes the deviation in percentage between the WWRP and the forklift multibody model. The maximum deviation present is 1.26% in the z coordinate of CoG at MLH. The WWRP is an analytical program that calculates the listed values for each truck based on a large data set of the available trucks. It calculates the mass and the CoG coordinates based on simplifications. For instance, WWRP assumes the chassis of the truck as a single body, which includes the engine, transmission, driver cabin and other components as one lumped mass. However, the model has the mass of the listed components situated exactly at the CoG locations calculated via CAD software. This could be a possible reason explaining the difference comparing the WWRP and model results.

The differences seen between the WWRP and the model were minor and zero deviations can be obtained by iterating some of the CoG locations. However, tuning and iterating CoG locations would cost time and is not considered to be scientific research. On the other hand, these values are close to the WWRP calculations with a maximum deviation of less than 2%. Therefore, the validation process is continued with the ISO 22915 verification of stability tests being simulated virtually explained in the next section.

5.2 ISO 22915: verification of stability tests

As discussed in Section 2.2, the ISO 22915 verification of stability is standard with minimum requirements that a truck must meet to be allowed to operate commercially. Therefore, these tests are conducted for every truck positioning the truck on a tilt table. The slope in percentage at which the truck starts to tip/roll over is noted and then compared to minimum requirements specified by ISO. These tests are replicated in the Simscape multibody environment and are used as a means to validate the model.

The slope requirements of the ISO and the stability limits calculated by WWRP are listed in Table 2.1 and can be used to determine the minimum tilt angle of the platform. The tilt angle (θ) by which the platform should be tilted to achieve the required slope percentage (s) can be determined by the following expression:

$$\theta = \text{atan}(\frac{s}{100}) \tag{5.1}$$

Table 5.2 lists the minimum required tilt angle of the platform for each test at which the forklift truck H9XD6 should remain stable. Furthermore, it also shows the tilt angles at

Table 5.2: ISO 22915: verification of stability details

Stablity Tests	Minimum requirement		Stability limit	
	Min. req. slope [%]	Angle [degree]	Slope [%]	Angle [degree]
Test 1	3.80	2.18	6.08	3.48
Test 2	18.00	10.20	24.97	14.02
Test 3	6.30	3.60	16.83	9.55
Test 4 WL	No std.	-	51.91	27.43
Test 4 ULT	50.00	26.56	94.14	43.27

which the truck is expected to become unstable according to the WWRP calculations.

The truck model is positioned on a platform that can tilt along the y axis of the vehicle with the help of a revolute joint in Simscape. The MATLAB script requires certain user-specified inputs such as the model name, lift height, mast inclination angle, inner steering tire angle and the stability platform angle to simulate the stability tests. Since there are two models for the two approaches for modeling tire behavior on an inclined surface, the model name depends on the approach used. In addition, specifying tire steering angle is only necessary for lateral stability tests whereas, in forward stability tests, the steering tire angle is 0. More information regarding model simulation can be found in Appendix A.

The simulations are performed until the respective wheel looses contact with the ground depending on the stability tests as described in Section 2.2. For example, while simulating test 1 concerning forward stability, the vertical force on the rear tires are monitored and as soon as they loose contact with the ground, the simulation is stopped and it is concluded that the truck has reached its stability limit.

In test 1, the carried load is set at a height of 4.675 meters. The mast inclination angle and steer tire angle are both maintained at 0 degrees. The simulation for forward stability test 1 is conducted using the two approaches outlined in Section 4.2.3. The results of this simulation are presented in Figures 5.1 and 5.2. Figure 5.1 depicts the behavior of the rear tire force as a function of tilt angle and illustrates that as the platform starts to tilt, the rear tire load starts to decrease. Notably, the rear tires lose contact with the ground earlier in approach 1, which involves the utilization of bushing joints, compared to the MF tire block approach. Figure 5.2 shows the input provided to the stability platform in Simscape which

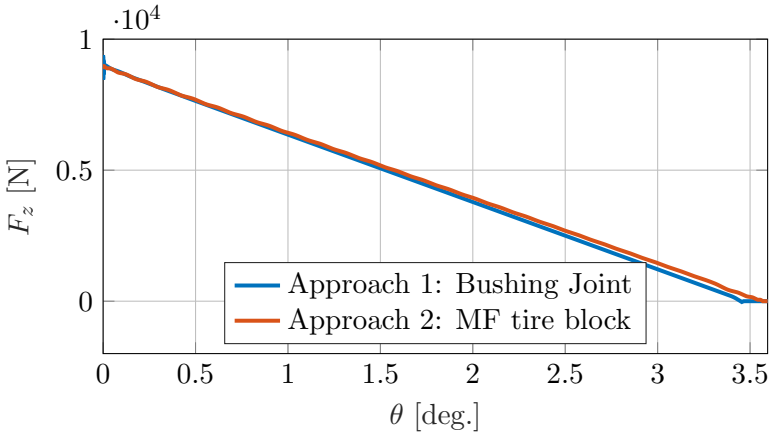

Figure 5.1: ISO stability test 1: rear tire forces

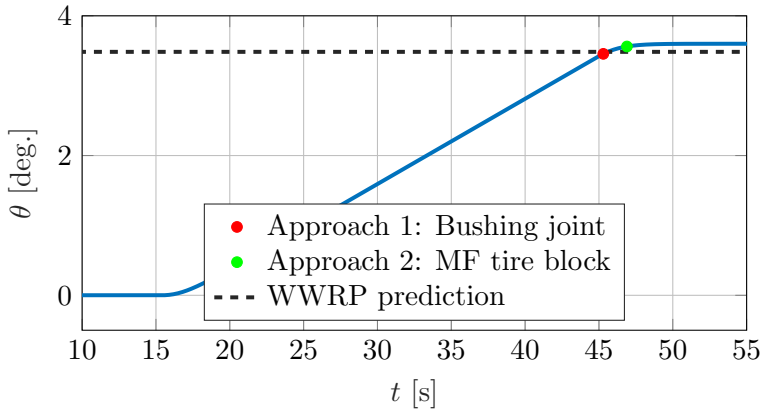

Figure 5.2: ISO stability test 1: platform tilt angle

gradually increases and attains a constant value of 3.60 degrees. For approach 1, the truck approaches instability at 3.46 degrees which aligns closely to the predicted WWRP stability limit of 3.48 degrees. In the case of approach 2, the platform angle measures to be 3.56 degrees when the tires loose contact from the ground.

Analysis of CoG position in the stability triangle

As mentioned under the stability concepts in Section 2.1, the CoG should remain inside the stability triangle to ensure that the truck is stable in a static situation. Since the ISO 22915 verification of stability tests are static and a longitudinal load transfer from the rear towards the front is observed in case of test 1, the CoG position must be on the border of the stability triangle at the time when the rear wheels loose contact with ground. This is also the point where the resultant force on the CoG points straight to the stability triangle boundary. Figure 5.3 shows the stability triangle for the lift truck H9XD6 where AB is the boundary for forward stability and AC and BC are the boundaries which account for lateral stability. The CoG position of the truck loaded with a maximum capacity of 8860 kg at MLH standing still on a flat surface is depicted by the red marker in Figure 5.3. The blue marker depicts the CoG position when the truck has reached its stability limit after the platform is tilted. Since test 1 accounts for forward stability, it is evidently shown that when the truck reaches its stability limit, the CoG is near the boundary of the stability triangle.

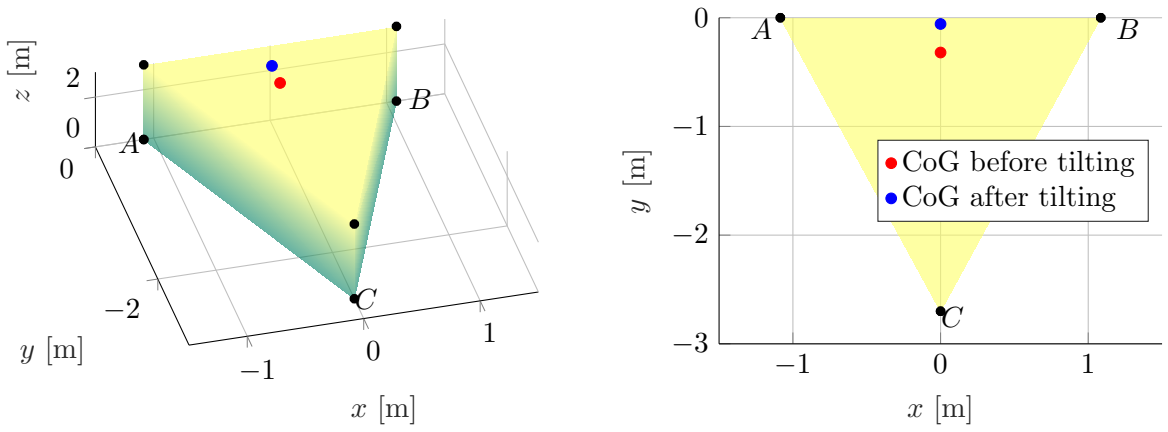

Figure 5.3: ISO stability test 1: CoG position in stability triangle

Table 5.3: ISO 22915: verification of stability Results

Stability Tests	Min. req. Degree	Platform angle at stability limit [Degree]		
		WWRP Calculation	Approach 1: Bushing joint	Approach 2: MF Tire block
Test 1	2.18	3.48	3.46	3.56
Test 2	10.20	14.02	12.40	13.23
Test 3	3.60	9.55	9.03	8.93
Test 4 WL	No std.	27.43	26.36	22.08
Test 4 ULT	26.56	43.27	40.43	41.43

The two approaches used to model contact between the tire and the ground on an inclined surface gave similar results. Similarly, the other ISO 22915 stability platform tests were performed and are discussed in Appendix C. Table 5.3 presents the results obtained with both approaches. The results obtained by the two approaches show a fair correlation with the WWRP calculations and satisfy the minimum ISO requirements. Apart from some minor deviations, a maximum deviation of 6% is observed after comparing the results. As a possible explanation, the WWRP also takes the mast deflection into account, however, in the multibody model the mast is treated as a rigid body.

5.3 Validation using dynamic tests

After completing the static evaluation of the multibody forklift model, dynamic tests are conducted to validate the lateral, longitudinal and vertical dynamics of the model. In this section, first, the instrumentation used in the dynamic tests is discussed, followed by the criterion to define the model accuracy in subsection 5.3.3. Subsections 5.3.4 and 5.3.5 discuss the procedure and results obtained in the steady-state circular test and the test involving acceleration-deceleration and change of direction, respectively.

5.3.1 Test equipment and setting

The forklift H9XD6 is equipped with two IMU sensors also known by the name Transportation Attitude Reference Sensor (TARS), as shown in Figure 5.4. The TARS-IMU is a sensor designed for heavy-duty vehicles to record vehicle angular rate, acceleration and inclination along all three perpendicular axes. The first sensor is located along the symmetry line of the x axis on top of the inner mast to consider the effect of carry height and deflection of the mast. The position of the sensor is denoted by 1 in Figure 5.4. The second sensor was

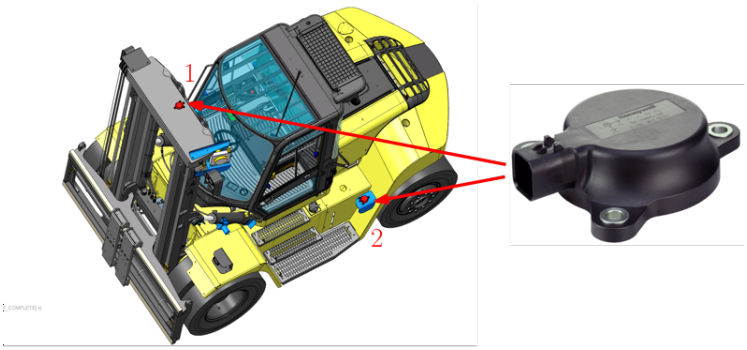

Figure 5.4: TARS- IMU sensors located on the forklift truck

favoured to be located on the CoG location of the basic truck without the front-end assembly. However, due to space constraints, it is situated at the position denoted by 2 in Figure 5.4. In addition, a string potentiometer is mounted in the center of the rear axle where the steering cylinder is located. This sensor captures the steering cylinder displacement as a function of time. By knowing the steering cylinder displacement, the steering tire angles can be calculated with the help of the steering geometry of the truck.

The steady-state and dynamic maneuver tests are conducted on an asphalt road assuming the coefficient of friction equal to 1. The road surface is not flat and has an inclination slope of approximately 1% to evacuate water in rainy situations. The vehicle velocity, the brake pedal position, and the steering cylinder displacement are extracted from the Controller Area Network (CAN) of the truck. The signals obtained from the CAN bus are filtered to remove high frequency noise before the simulation. This is achieved by filtering the inputs with a low pass filter with cut off frequency of 10 Hz using the MATLAB function *Filtfilt* and *Butterworth*. The obtained filtered signals of the velocity, brake pedal position and steering cylinder stroke are provided to the multibody model as inputs.

The solver settings affect the accuracy of a model. A variable time step solver, ODE 45, is used with a maximum time step of 10 milliseconds. The absolute and relative tolerances are also fine-tuned and are kept as 10^{-4} and 10^{-6}, respectively. By keeping the mentioned values for the absolute and relative tolerances the absolute and relative errors are minimum.

The longitudinal and lateral accelerations along with yaw rate are used to compare model and measured data. The signals measured from the truck CAN bus are filtered using *Filtfilt* and *Butterworth*. To obtain listed signals in MATLAB, transform sensor blocks are positioned at the same locations as on the physical truck, as illustrated in Figure 5.4. The signals from the transform sensor block are not filtered as the model does not contain sensor noise. However, these signals require adjustment in order to get the same response as the measured signals from the TARS-IMU sensors. The subsequent subsection elaborates on the gravitational correction applied to the transform sensor signals in MATLAB.

5.3.2 Correction of simulation output signals

In the Simscape multibody model, a transform sensor block is used to measure the vehicle accelerations along with roll, pitch and yaw rate with respect to a particular frame. Therefore, the base frame of the transform sensor is connected to the world frame in the model and the non-rotating follower frame is connected to the locations 1 & 2 as illustrated in Figure 5.4. It is observed that the simulation outputs do not include the gravitational component. For example, at standstill the simulation output resulted in a value of 0 m/s^2 for the acceleration along the z axis (a_z) instead of 9.81 m/s^2 obtained from an accelerometer. It is concluded that the transform block does not measure the difference between the inertial and gravitational acceleration, as done in the real vehicle IMU sensors. The accelerations measured by an IMU sensor are given by the following expression discussed in the study of Baaij [9]:

$$\vec{f} = \vec{a} - \vec{g}, \tag{5.2}$$

where $\vec{f}$ is the measured acceleration by an IMU sensor, $\vec{a}$ is the inertial acceleration and $\vec{g}$ is the gravitational acceleration.

The following solution is implemented in the Simscape model using the rotation measurements of the vehicle. The rotation measurements along each axis are represented in the form of a rotation matrix defined with respect to the world frame. Therefore, to attain the rotation matrix in the vehicle frame, it has to be transposed. The transposed rotation matrix is multiplied with the gravitational acceleration to attain the proportion of gravitational force with respect to the rotation angle. The result is then added to the accelerations of the transform sensor block. This is shown by the following expression:

$$\begin{bmatrix} a_{x,\text{IMU}} \\ a_{y,\text{IMU}} \\ a_{z,\text{IMU}} \end{bmatrix} = \begin{bmatrix} a_{x,\text{sensor}} \\ a_{y,\text{sensor}} \\ a_{z,\text{sensor}} \end{bmatrix} - \begin{bmatrix} r_{xx} & r_{xy} & r_{xz} \\ r_{yx} & r_{yy} & r_{yz} \\ r_{zx} & r_{zy} & r_{zz} \end{bmatrix}^{\top} \cdot \begin{bmatrix} 0 \\ 0 \\ g \end{bmatrix} \tag{5.3}$$

where a_x, a_y and a_z are the accelerations in x,y and z directions. This way the accelerations from transform sensor block are corrected by adding the gravitational components. An in depth validation can be found in Appendix B. The result obtained is compared with the accelerations measured by the TARS-IMU sensors mounted on the truck.

5.3.3 Quantification of model results

To compare the model predictions against the measured signals, a criterion is developed using the research of Jan Loof [14] and Backhuijs [13]. The criterion consists of three metrics that indicate the correlation between two signals based on different mathematical properties.

The first metric is Pearson's correlation coefficient which is used to determine a linear correlation between the measured and the simulated signal. The Pearson's correlation coefficient represented by R is calculated by the following expression:

$$R = \frac{\sum_{i=1}^{n}(x_i - \bar{x})(y_i - \bar{y})}{\sqrt{\sum_{i=1}^{n}(x_i - \bar{x})^2}\sqrt{\sum_{i=1}^{n}(y_i - \bar{y})^2}}, \tag{5.4}$$

where x is the measured signal, y is the simulated signal, $\bar{x}$ and $\bar{y}$ are the respective means of the two signals and n is the number of samples.
The above expression results in a number between -1 and 1 to denote the correlation between the two measured signals. R = 0 denotes there is no correlation between the two signals, R = 1 denotes a strong positive correlation and R = -1 denotes a strong negative correlation. However, there is a shortcoming in this method that it does not consider the offset which might be present between the two compared signals. Therefore, using only Pearson's correlation coefficient to determine the result quality may give a false indication of model accuracy.

To solve the shortcoming of Pearson's correlation coefficient method, an offset error is calculated which is defined as the difference between the means of the two signals normalized over the range of the measurement signal. Normalizing the error facilitates the comparison between signals with different scales. The offset error (ϵ) is given by the following expression:

$$\epsilon = \frac{\bar{x} - \bar{y}}{|\max(x) - \min(x)|} \cdot 100\% \tag{5.5}$$

Apart from Pearson's correlation coefficient (R) and offset error (ϵ), the Normalised Root Mean Square Deviation (NRMSD) is also used to measure differences between two signals.

The NRMSD is always non-negative and a value equal to 0 represents a perfect correlation between the two signals. The NRMSD is calculated by the following expression:

$$\text{NRMSD} = \sqrt{\frac{\frac{\sum_i^n (x_i - y_i)^2}{n}}{|\max(x) - \min(x)|}} \tag{5.6}$$

The above-mentioned three metrics are calculated to quantify the differences between measurements and simulation model. Although, these methods do not consider the phase shift. If there exists a slight phase shift between the two compared signals, the correlation coefficients derived can be misleading. Therefore, this is a limitation to these criteria used to assess the resulting quality. Observing the quality of the measured signals and taking reference from Loof [14] and Backhuijs [13], the following criterion is developed to classify the results as being accurate:

- $R \geq 0.85$
- $-10\% < \epsilon < 10\%$
- $NRMSD < 0.2$

5.3.4 Steady state circular driving

The steady-state circular driving test is performed to evaluate the lateral and yaw dynamics of the forklift. In this test, the fork height of the truck is set to 0.5 meters above the ground and the mast is vertical i.e. at a 0-degree inclination angle. A circle with a turning radius of 4 meters is marked on the ground and the truck driver is instructed to maintain a constant steering angle to follow the circle with the inner front tire as close as possible to the marked line. Since the truck has been functioning for four years, components such as bearings and steering arms have developed some offsets and errors due to wear. Hence, it is difficult to maintain a steady-state circle by keeping a fixed steering angle. Therefore, the driver has to make corrections to the steering angle whenever the truck goes off the intended path. To ensure that the truck is running at a constant velocity, the cruise controller is set to 3 km/h. Steady-state circular tests are performed for both left and right-hand turns and similar results are obtained. Therefore, results for the steady-state circular test for the left turn are presented next and for right turn can be found in Appendix C.

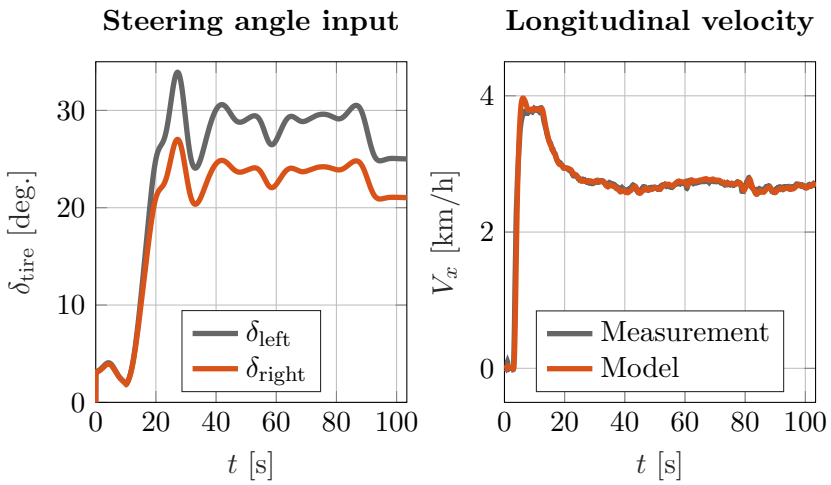

Figure 5.5: Steady state circular driving: Simscape model inputs

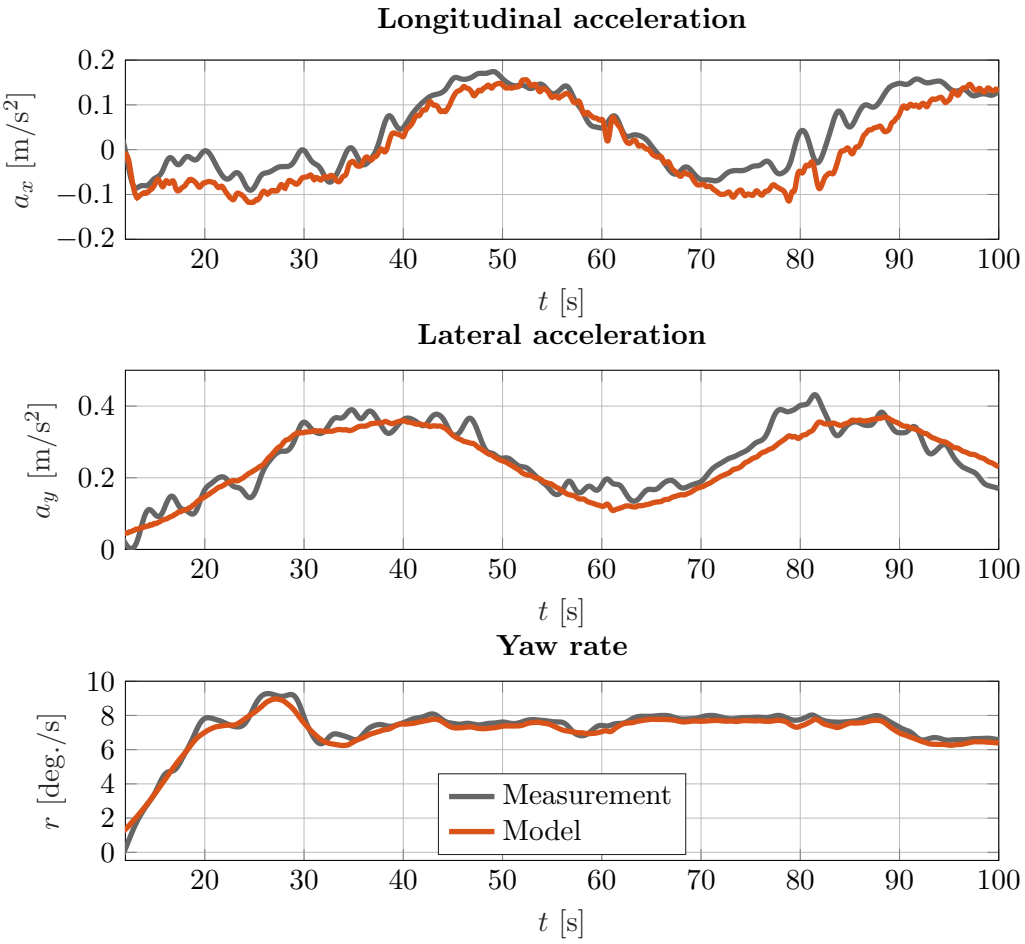

Figure 5.6: Steady state circular driving: Results

The vehicle velocity and the steering angles are provided as inputs to the Simscape model, as shown in Figure 5.5. The steering angles for the left and right tires are calculated with the help of the measured steering cylinder displacement. In the steering angle input plot shown in Figure 5.5, the left tire turns at a greater degree as compared to the right tire depicting Ackermann steering geometry as implemented in the Simscape model.

The longitudinal velocity provided to the cruise controller is 3 km/h, but the reference velocity measured from the CAN bus remains less than 3 km/hour as shown in Figure 5.5. It is concluded that the controller used to maintain constant velocity does not perform accurately and only allows the velocity to be 90% of the reference velocity provided as input. However, the model tracks the provided reference velocity very well using the cruise controller.

The longitudinal and lateral accelerations along with the yaw rate are used to validate the multibody model. Figure 5.6 shows the three signals measured by the IMU located on the truck body compared with the simulated data. Signals measured by the IMU located on the top of the mast also depict similar behavior. In the case of steady-state circular driving, the accelerations of a vehicle are expected to be constant whereas Figure 5.6 shows a wavy nature

Table 5.4: Steady-state circular driving: correlation coefficients

Signal	R	ϵ	NRMSD
Velocity (V_x)	0.96	0.18	0.05
Longitudinal acceleration (a_x)	0.86	5.33	0.11
Lateral acceleration (a_y)	0.89	3.36	0.10
Yaw rate (r)	0.91	6.45	0.09

for the lateral and longitudinal accelerations. This is caused by the 1 % inclination angle present at the ground surface. As a result, the sensor is slightly inclined with respect to the world frame. Therefore, the IMU measures an extra component of gravity, while measuring vehicle accelerations as explained in subsection 5.3.2, causing this wavy nature. In Simscape, the ground level is tilted by an angle of 0.7 degrees to achieve the results shown in Figure 5.6.

Table 5.4 presents the correlation coefficients calculated to quantify the results obtained. The obtained correlation coefficients are well within the accuracy criterion described in subsection 5.3.3. Hence, it is concluded that the model can predict the lateral and yaw dynamics in a steady state circular test as well.

5.3.5 Test involving acceleration-deceleration and change in direction

The model is validated with a test in which the longitudinal, lateral and vertical behavior of the model is evaluated. The test is conducted such that it includes acceleration, cornering and deceleration to get an understanding of the overall performance of the model. The Simscape model is fed with the velocity and the steering cylinder displacement measured during actual test. In addition, since this test involves rapid deceleration, the brake pedal position input is also provided to the Simscape model. Figure 5.7a shows the path followed by the forklift truck which shows that the test consists of right as well as left turn. Furthermore, Figure 5.7b illustrates the zones where the truck was accelerated and braked shown by I and III, respectively.

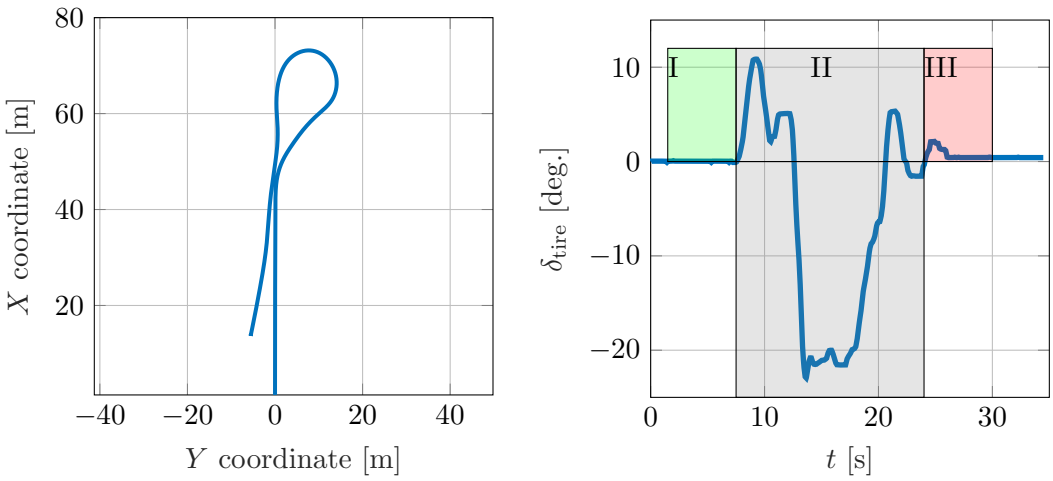

(a) Path followed **(b)** Acceleration and deceleration zones

Figure 5.7: Dynamic validation test

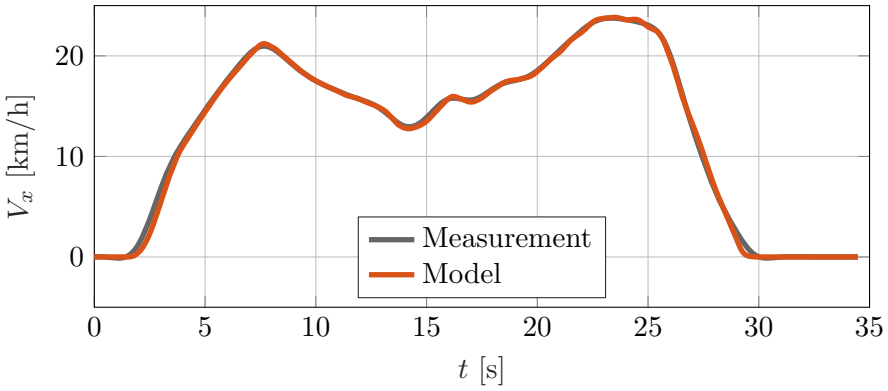

Figure 5.8: Dynamic test: reference and simulated longitudinal velocity of the forklift

As shown in Figures 5.7a and 5.7b, the forklift moved along a straight path with the maximum achievable acceleration until it approached a right turn. The turning zone, depicted by II, encompassed the sequence where the forklift underwent a right turn followed by a left turn. Subsequently, within zone III, the forklift entered a braking phase, ultimately bringing it to a complete stop. Figure 5.8 shows the measured and the simulated velocity of the forklift, which appear to correlate remarkably well due to the integration of the brake input within the Simscape model. It is noted that, if necessary in the future, the development of a brake controller could be considered in cases where the accuracy of the brake pedal position input is compromised. However, the current brake input mechanism exhibits satisfactory performance for the present study's purposes.

Figure 5.9 presents the comparison of the measured and simulated lateral acceleration of the dynamic test which involved acceleration, turning and deceleration. The theoretical validation conducted by the bicycle model in Chapter 3 led to an insight that the lateral acceleration first builds up in an opposite direction and switches the direction while going through a corner. This is also evidently seen in the plot for lateral acceleration in Figure 5.9 where at time instant $t = 7.5$ s, the lateral acceleration is positive while turning right and then switches the direction and attains a negative sign. The yaw rate and the longitudinal acceleration are shown in Figure 5.10 which also correlate remarkably well. The correlation coefficients for this test are listed in Table 5.5 which show that the model is capable of accurately predicting the behavior of the forklift H9XD6.

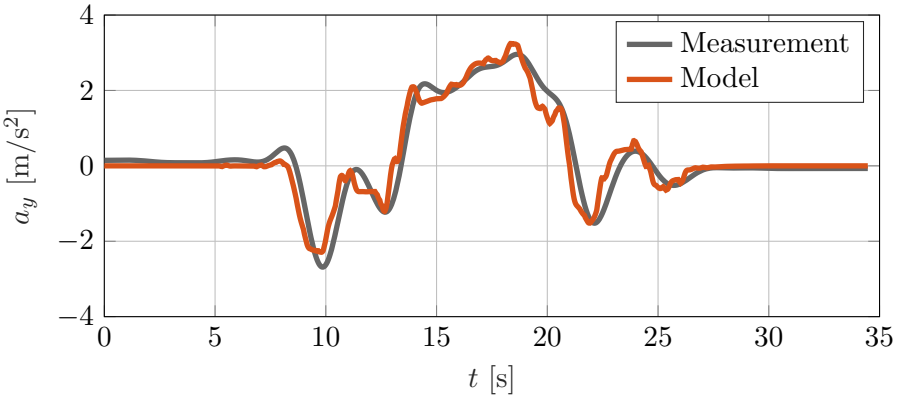

Figure 5.9: Dynamic test: lateral acceleration

Table 5.5: Dynamic test: correlation coefficients

Signal	R	ϵ	NRMSD
Velocity (V_x)	0.99	0.17	0.01
Longitudinal acceleration (a_x)	0.94	2.40	0.06
Lateral acceleration (a_y)	0.94	2.32	0.07
Yaw rate (r)	0.99	0.07	0.03

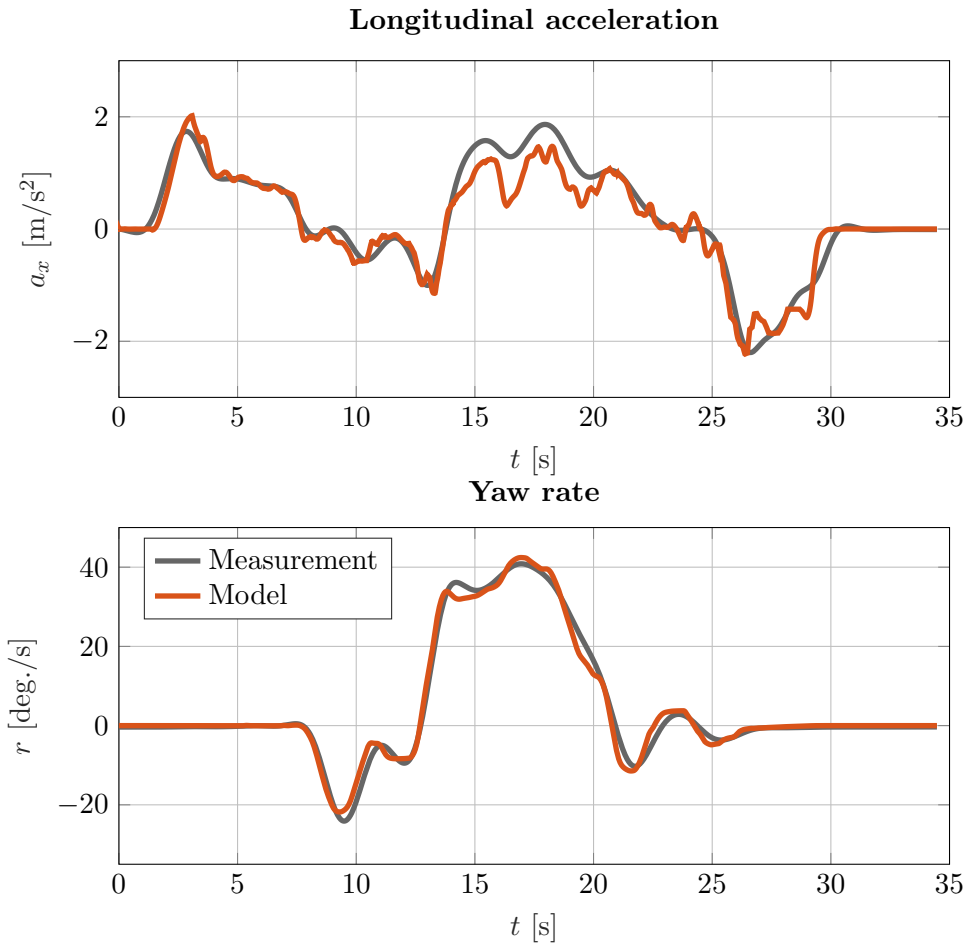

Figure 5.10: Dynamic test: longitudinal acceleration and yaw rate

5.4 Summary

This chapter discussed the validation process of the forklift multibody model developed in Simscape. The comprehensive validation procedure highlights the reliability and accuracy of the developed forklift multibody model. Thereafter, the developed multibody model is used to simulate critical scenarios of instability which are discussed in the next chapter.

Chapter 6

Identification of Critical Scenarios

Following the development and validation of the forklift multibody model in Simscape, several critical instability scenarios are identified through simulations involving various hazardous situations. This chapter presents the simulation outcomes of these scenarios, wherein the forklift approaches its stability limit. The results consist of upper limits and boundary conditions to velocities and accelerations, beyond which the forklift is prone to tip or roll over. The primary objective of this chapter is to identify scenarios which should be avoided in real life.

It is necessary to classify metrics that serve as indicators for identifying critical scenarios. As discussed in Section 2.4, the Rollover Index (RI) is the chosen metric for this research, to identify the point where the truck initiates to roll over. The RI also referred to as Lateral Load Transfer Ratio (LLTR) is defined by Yunbou [16], through the following expression:

$$RI = \frac{F_{z\text{Left}} - F_{z\text{Right}}}{F_{z\text{Left}} + F_{z\text{Right}}}, \tag{6.1}$$

where $F_{z\text{Left}}$ is the sum of vertical forces on the left tires and $F_{z\text{Right}}$ is the sum of vertical forces on the right tires. As inferred from (6.1), the RI is 0 when there is no load transfer as the load on each side is equal considering the vehicle is symmetric. The RI can have extreme values of $+1$ or -1 either the right or left tires loose contact with the ground. For this research, a scenario is identified as unstable when the RI value attains the threshold of ± 1, signifying that the wheels from one side have lost contact with the ground.

Similar to RI, metric for predicting forward stability is formed known as the Tipover Index (TI). The TI is defined by the following expression:

$$TI = \frac{F_{z\text{Front}} - F_{z\text{Rear}}}{F_{z\text{Front}} + F_{z\text{Rear}}}, \tag{6.2}$$

where $F_{z\text{Front}}$ and $F_{z\text{Rear}}$ are the combined vertical tire forces on the front and rear axle, respectively. The truck does not have equal loads on the front and rear which leads to the TI being equal to 0.83 when the truck is standing still with maximum load of 8860 kg at MLH. This is already high and the truck has small stability margins; nevertheless, a particular scenario is only considered unsafe when the rear axle completely looses contact with the road, signifying, TI = 1.

Some of the scenarios where a forklift can develop high accelerations which force the RI and TI to surpass the criterion mentioned above are studied in the research of Larsson [15].

Additional research on such dangerous scenarios where the forklift is prone to tip or roll over is conducted by interacting with the forklift developers at Hyster-Yale Group. During this interaction, various validation and test engineers were interviewed and their views on critical scenarios were considered. Based on the information gathered, four critical instability scenarios are simulated virtually which have a high probability of occurrence. Comprehensive explanations and the outcomes of each critical scenario are elaborated upon in Sections 6.1 to 6.4.

6.1 Critical scenario 1: Approaching a stack

This section elaborates a critical scenario where a forklift with maximum load is approaching a stack to unload the carrying payload. The payload has to be stacked at maximum height therefore, the forklift is carrying the payload at Maximum Lift Height (MLH). When the lift truck approaches the stack, the truck driver has to decelerate to stop the forklift in front of the stack. It has to be noted that the truck driver should not brake with a high deceleration otherwise the lift truck can tip over. The main aim behind simulating this scenario is to identify the speeds above which the truck reaches its stability limit for different brake pedal positions. In this scenario, three brake pedal positions are considered where the brake pedal is actuated to 30%, 50% and 100% of the braking capacity within 1 second. Since the reaction time of a young attentive driver, ready to brake is 0.6 seconds [26], the time of actuation is rounded up to 1 second considering other actuation delays as well. The brake input for the simulation is shown in Figure 6.1a.

Figure 6.2 depicts the stability metric TI for the critical scenario 1 simulated at the respective brake pedal positions. While simulating these braking scenarios it is found that there are situations when the rear tires loose contact with the ground but return back although the TI has reached the threshold value of 1. In Figure 6.2, the TI starts from 0.83 and returns to the same value but with oscillations. The rear wheels loose contact from the ground, but eventually return back to the ground and the vehicle bounces on the tires. The time instant where the rear wheels hit the ground surface, the rear axle is loaded again and there occurs a large load transfer with a pitching motion of the truck. This is shown by the oscillations of the TI in Figure 6.2.

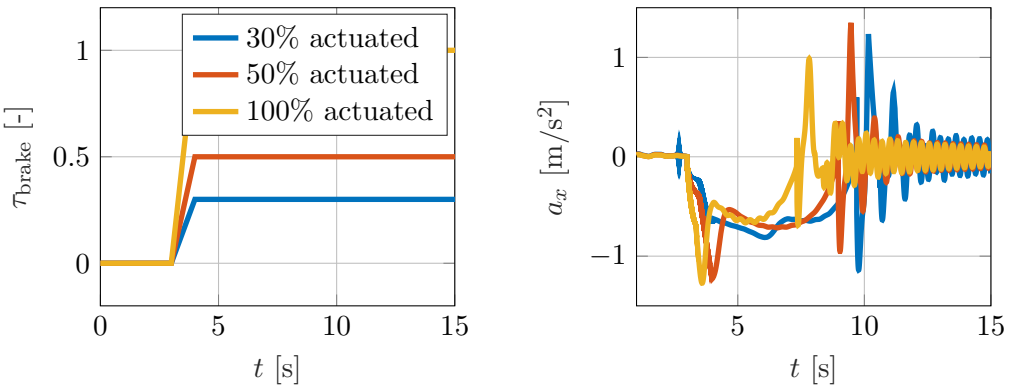

(a) Brake input **(b)** Longitudinal acceleration

Figure 6.1: Critical scenario 1

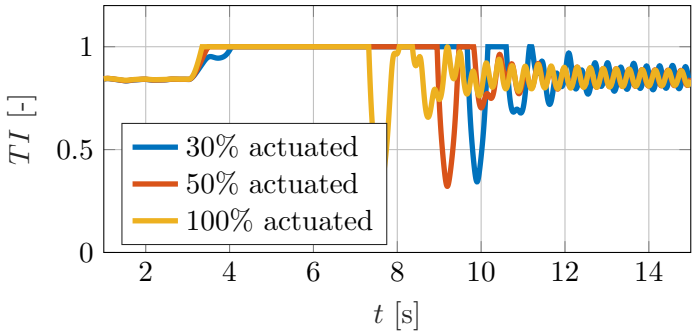

Figure 6.2: Critical scenario 1: Tipover Index

This scenario is simulated until the truck reaches the '*point of no return*' where the truck completely tips over if a larger velocity is provided. Figure 6.1b shows the longitudinal acceleration with respect to time. Since the brake actuation is completed at 4 seconds, the upper bounds to longitudinal deceleration are obtained at $t = 4$ seconds. When the brake pedal is fully actuated, the truck completely tips over above 2.7 km/h and the maximum deceleration achieved is -1.27 m/s^2. Furthermore, when the brake pedal is actuated by 50% and 30%, the truck reaches its point of no return above 3.9 km/h and 7.5 km/h achieving a deceleration of -1.22 m/s^2 and -0.8 m/s^2, respectively. Simulations were also conducted by reducing the brake actuation time resulting in lowering the values of critical velocities.

6.2 Critical scenario 2: Stack exit

One of the scenarios that takes place in a warehouse or at a transportation port is that the forklift has picked up or dropped the payload at Maximum Lift Height (MLH) successfully but it has to go in the reverse direction while turning. The truck drivers apply the maximum steering angle, while driving in reverse direction. This may cause the forklift to roll or tip over depending on the speed and the load carried. Therefore, two situations are considered when simulating this type of a scenario in the virtual environment. First situation is in which the forklift is loaded with maximum load at MLH and starts to drive in reverse while turning at constant speed. Second in which the payload is eliminated, but the mast is still at MLH and the truck is given the same steering input. Figure 6.3 depicts the steering input provided to the forklift in both the situations, which reaches the maximum steering angle within a time frame of 5 seconds and is maintained constant afterwards. The aim of this simulation is to find the critical velocity and accelerations at which the truck would tip or roll over in these two situations.

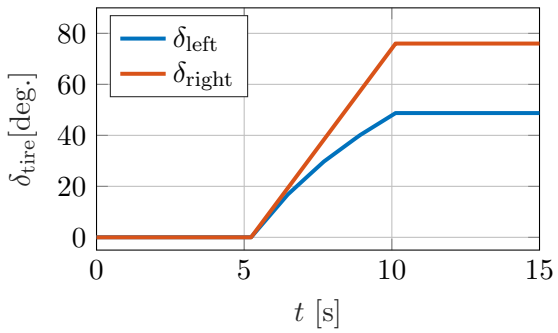

Figure 6.3: Critical scenario 2: steering input

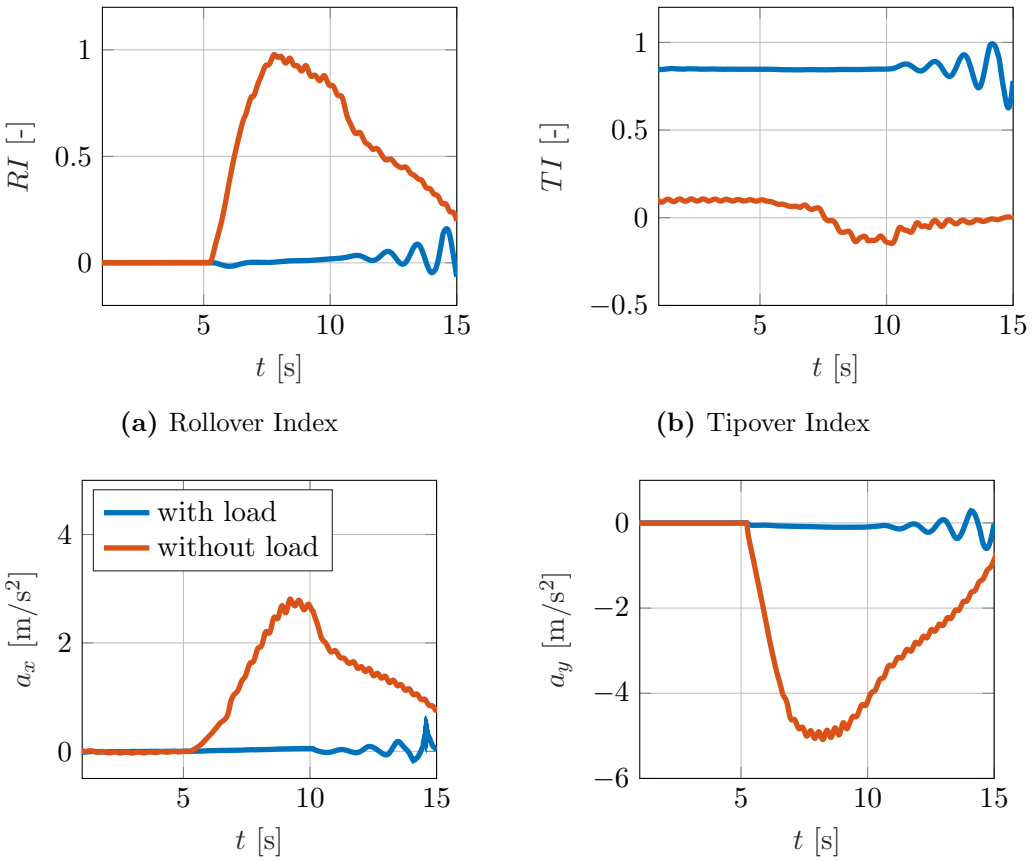

(a) Rollover Index

(b) Tipover Index

(c) Longitudinal acceleration

(d) Lateral acceleration

Figure 6.4: Critical scenario 2

Figures 6.4a and 6.4b depict the stability metrics calculated while simulating critical scenario 2. In the first situation, where the truck is driving in reverse with maximum load at MLH, the critical velocity at which the truck becomes unstable is 1.8 km/h. Since, the truck is loaded with maximum rated load, the truck already has a high TI. At $t = 14$ seconds, the TI reaches the threshold value of 1 signifying rear wheels lift off in Figure 6.4b. However, RI shown in Figure 6.4a, is nowhere close to the threshold for the first situation. Hence, observing the behavior of TI, the truck is predicted to tip over above 1.8 km/h. Figure 6.4c and 6.4d depict the longitudinal and lateral acceleration whose critical values at $t = 14$ seconds are found to be 0.5 m/s^2 and 0.27 m/s^2, respectively.

In the second situation, where the load is eliminated but the mast is still elevated at MLH, the stability limits are found to be relaxed. The truck can be driven at higher speed but not more than 22 km/h as the Rollover Index has almost reached the threshold value at approximately $t = 8$ seconds as seen from the Figure 6.4a. Since the payload is eliminated in this situation, the TI is well within the boundary depicted in Figure 6.4b. Figure 6.4c and 6.4d depict the longitudinal and lateral acceleration whose critical values at $t = 8$ seconds are found to be 2.8 m/s^2 and 5 m/s^2, respectively.

6.3 Critical scenario 3: Ramp steer response

Predicting the behavior of a lift truck on a ramp steer would be of great importance in real life. For example, a forklift driver, driving with maximum capacity encounters a pedestrian suddenly in front of the truck, either the brakes should be applied immediately or the forklift should be steered rapidly away from the pedestrian to avoid a collision. The option of braking immediately has already been proven to be dangerous from the simulation results for critical scenario 1 discussed in Section 6.1.

Therefore, a ramp steer scenario is simulated for the forklift H9XD6 carrying the rated load at Maximum Lift Height (MLH) at top speed of 31 km/h. The forklift is subjected to a ramped steering angle starting at $t = 4$ seconds as shown in Figure 6.5. The ramp input is defined assuming all actuation delay and driver reaction time accounting to 1 second as done in critical scenario 1. The simulations are performed with a steering angle equal to 1 deg. and then the steering angle is increased until the stability metrics reach their threshold limits. It is observed that when the truck is subjected to a step input of 9 deg., the truck almost reaches its stability limits. Figure 6.6a shows the stability metric RI during the simulation which after 9 deg. of step input, settles above 0.8. For simplicity, the increment of the steering angle is assumed to be 1 deg. and when a steering input greater than 9 deg. is given, the RI attains a value of 1 and the wheels loose contact from the ground. Therefore, the critical steering angle for this scenario is 9 deg. and the critical lateral acceleration is observed to be 2.6 m/s^2 from the Figure 6.6b.

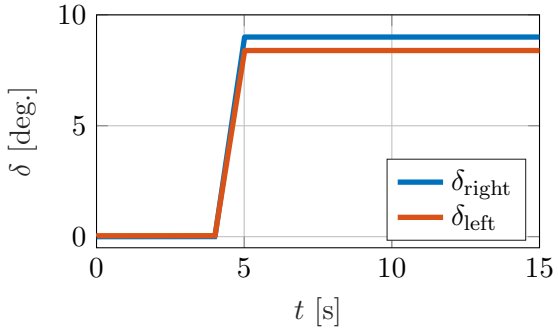

Figure 6.5: Critical scenario 3: steering input

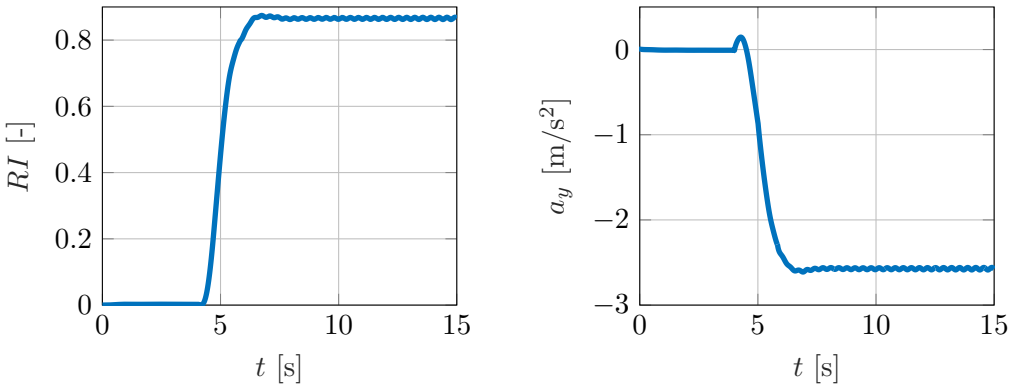

(a) Rollover Index **(b)** Lateral acceleration

Figure 6.6: Critical scenario 3: outputs

6.4 Critical scenario 4: 90 degree turn

According to the European Standard EN 16203 [27], dynamic tests for the verification of lateral stability are specified for counterbalanced lift trucks with a rated capacity up to 5000 kg. In this test, a forklift is driven at 90% of its maximum velocity with no load and is suppose to complete a 90 degree turn without the front inner wheel lifting off the ground surface. More details to this test are mentioned in the document EN 16203 [27].

However, the Hyster forklift H9XD6 has a rated capacity of 8860 kg and does not fall in this category. According to the current legislation, the EN 16203 lateral stability test is not compulsory for the truck analyzed in this thesis. However, the European Standards are becoming particular about the safety of big trucks and there is a possibility in the near future that a similar test might be included for the Hyster H9XD6 forklift. To conduct a test involving a 90 degree turn at 90% of the truck's maximum velocity, might be a dangerous situation and the truck will have to be equipped with safety jigs, such that it does not tip/roll over. To avoid conducting this test physically, it is simulated virtually with the developed multibody model and stability limits are identified.

To identify stability limits, a simulation with a 90 degree turn of turning radius approximately 9 meters, as shown in Figure 6.7a, is performed at 90% of the truck's maximum velocity at carry height with no load. Figure 6.7b depicts the RI which evidently shows that the truck proves to be safe as no wheel lift is detected at 27 km/h. A second simulation in which the truck is driven at its top speed of 31 km/h is presented where it is again found that the truck remains stable. Since, the truck is stable in this test, another simulation is performed in which the fork height is increased from carry position to 4.675 meters above the ground (MLH) with maximum load. This has a significant impact on the CoG of the truck being raised. Hence the maximum velocity at which the truck can follow the 9 meter turning radius path without rolling over is reduced to 23 km/h.

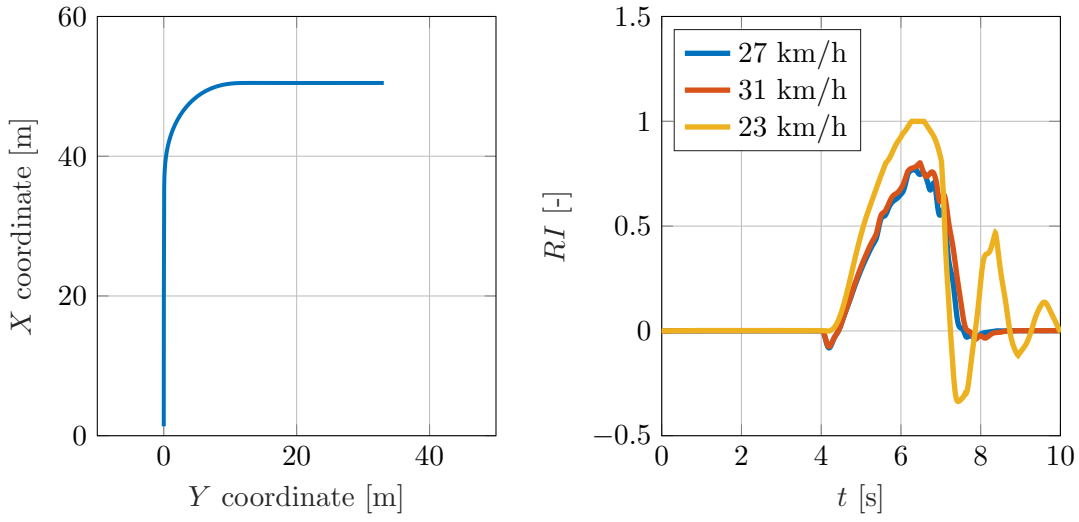

(a) 90 degree path **(b)** Rollover Index

Figure 6.7: Critical scenario 4

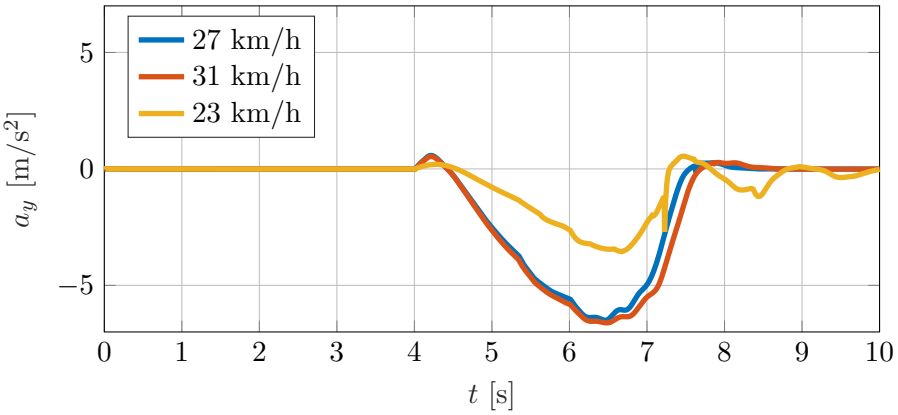

Figure 6.8: Critical scenario 4:Lateral acceleration

As discussed, the two simulations performed at carry height are stable and the respective RI's are below the the threshold value. However, the lateral accelerations experienced by the truck are higher in the first two simulations as shown in Figure 6.8. Further, results of the third simulation are presented where the respective RI shows that the truck looses road contact, but does not rollover completely and returns back to stable condition. Therefore, it is predicted that if the loaded truck is operated at a speed greater than 23 km/h at MLH for following a 90 degree path of turning radius 9 m, it may lead to a rollover.

6.5 Boundary conditions

After simulating the four scenarios explained above, critical values for parameters such as velocity, lateral and longitudinal accelerations have been determined. The threshold values for each scenario beyond which the truck is at risk of a tip or roll over, are presented in Table 6.1. The table explains the scenario in brief, gives information about the fixed inputs and variable inputs while the scenarios were simulated. Finally, the last column of Table 6.1 depicts the critical velocities and accelerations for each scenario.

As can be seen, the critical values obtained for dynamic scenarios are different for each of the critical scenario. Depending on the inputs given to the truck, the values of critical velocity and acceleration change considerably.

Further, the critical values can be linked to the stability triangle discussed in Section 2.1. The resultant forces acting on the CoG of the truck change in dynamic situations. However, above these critical values, the resultant forces acting on the CoG of the truck, would meet the ground surface outside the stability triangle boundary as per the stability concept. This would eventually result in a tip or a roll over. Determining resultant forces acting on the CoG in dynamic situations is difficult, whereas, monitoring parameters such as velocity and accelerations is feasible. Therefore, these critical values can be used as threshold values to compare with the real-time velocity and acceleration measured by the forklift under different situations. This way warning systems can be developed to aware the driver of dangerous situations and enhance operational safety.

Table 6.1: Critical scenarios: boundary conditions

Critical scenario	**Fixed inputs**	**Variable input**	**Critical Value(s)**
Approaching a stack Detecting tip over due to provided braking torque	Load: 8860 kg Mast tilt: 0 deg. Lift height: 4.675 m (MLH)	Velocity Brake pedal input 30% actuated	V_x a_x V_x: 7.5 km/h a_x: -0.8 m/s^2
		50% actuated	V_x: 3.9 km/h a_x: -1.22 m/s^2
		100% actuated	V_x: 2.7 km/h a_x: -1.27 m/s^2
Stack exit Detecting roll over when driving and turning simultaneously in reverse	Mast tilt: 0 deg. Lift height: 4.675 m (MLH) Max. steering angle	Velocity Load Load: 8860 kg	V_x a_x a_y V_x: 1.8 km/h a_x: 0.5 m/s^2 a_y: 0.27 m/s^2
		Load: 0 kg	V_x: 22 km/h a_x: 2.8 m/s^2 a_y: 5 m/s^2
Ramp steer Detecting a wheel lift while giving a ramp steer input at max. velocity	Load: 8860 kg Mast tilt: 0 deg. Lift height: 4.675 m (MLH) V_x: 31 km/h	Steering angle	δ_{inner}: 9 deg. a_y: 2.6 m/s^2
90 degree turn Detecting a wheel lift while following a 90 degree turn	Load: 8860 kg Mast tilt: 0 deg. Lift height: 4.675 m (MLH) R: 9 m	Velocity	V_x: 23 km/h a_y: 3.48 m/s^2

Chapter 7

Conclusions & Recommendations

Observing the results of the simulated scenarios, critical values for velocity and accelerations are determined. This chapter highlights the overall conclusions drawn from this master's thesis and also presents recommendations to various items which require further attention.

7.1 Conclusions

Based on the model validation and results obtained, it is concluded that a trustworthy multibody model of the forklift H9XD6 has been created. The model is capable to conduct handling simulations which have been proven to align with measurements on the real vehicle. During the development and validation of the multibody forklift model, following specific conclusions are established:

- Dynamics of a rear-wheel steered vehicle were studied in this research by developing a dual steer bicycle model which resulted in interesting conclusions. It is concluded that the instantaneous center of rotation for a rear-wheel steered vehicle, is always located ahead of the front axle.
  The vehicle side slip angle for a rear-wheel steered vehicle always remains positive irrespective of the forward velocity. Furthermore, the lateral acceleration always builds up in the opposite direction of the turn and then switches direction.

- During the model development, the powertrain subsystem is designed as a diesel electric motor being a simplification of reality. Since the primary objective of the project focuses on vehicle dynamics and determining the vehicle response in different situations, it is concluded that the implementation of a simple powertrain is sufficient.

- Similar to the powertrain subsystem, the braking subsystem is also simplified in this research. The braking subsystem works on scaling the maximum brake torque using the pedal position profile. It was observed that the model is able to track the reference velocity quite well. Therefore, it is concluded that modelling the actual braking mechanism or developing a brake controller is not necessary.

- While comparing the static validation results obtained from the multibody model with the WWRP, small deviations were observed. WWRP being an analytical solution follows a simplified calculation method where various subsystems are lumped as a single body and results are generated. Whereas the multibody model has mass and inertia characteristics of each subsystem separately. This might be a possible reason for observing the deviations. It is to be noted, that the deviation between the two compared models is small.

- The multibody model is used to simulate the ISO 22915 stability platform tests with the two developed approaches for a non-rolling tire. Comparing the results with the WWRP, it is concluded that both approaches give results similar to the WWRP calculations.

  However, there were minor deviations while comparing the obtained results with WWRP. These also might arise from the fact that the multibody model is developed considering rigid bodies whereas the WWRP considers mast deflection at elevated heights.

- Based on the results obtained in the ISO 22915 stability tests, it was observed that even though the CoG of the truck was inside the stability triangle boundary, the truck tipped or rolled over. Therefore, it is concluded that only ensuring that the CoG of the truck is inside the stability triangle does not account for stability. It is crucial that the resultant force acting on the CoG meets the ground inside the stability triangle to ensure that the truck is stable.

- Typically, vehicle tests are conducted on a flat road surface not having any inclination angles resulting in constant accelerations in steady-state tests. However, while conducting steady-state tests for the forklift, it was observed that the ground surface was not completely flat and had an inclination angle of approximately 1% slope. The wavy trend seen in longitudinal and lateral acceleration is a cause of the additional gravitational component which exists due to the sloped road surface.

- For dynamic maneuvers of the forklift model, the Magic Formula tire force and torque block with altered tire characteristics of a commercial vehicle is used. Since the model results align with the measurements on real vehicle, it is concluded that these tire characteristics are a fair representation of the tires currently installed on the truck.

- In the final stage of the project, the developed and validated multibody model was simulated in scenarios which a forklift driver might encounter. Observing the results of the simulated scenarios based on day-to-day activities, it is concluded that the truck can reach its stability limits if operated carelessly.

- The critical values obtained based on the defined stability metrics are not the same for every critical scenario. It is also observed that even at small velocities and accelerations, the truck could lead to a tip or roll over. Therefore, it is concluded that the threshold values of lateral and longitudinal acceleration determined from steady state calculations do not apply in case of dynamic situations.

- Based on the stability metrics, the obtained threshold values of velocity and accelerations are the values beyond which the truck may lead to a tip or a roll over. These are linked to the stability triangle concept and it is concluded that the resultant force acting on the CoG of the truck would meet the ground surface outside the stability triangle boundary if these threshold values are surpassed. As a result, the truck would become unstable.

7.2 Recommendations

Though the modelling approach presented in this thesis has been applied successfully in identifying critical instability scenarios, there are some recommendations for future research:

- The multibody model uses the tire property file of a pneumatic tire which is different from the solid tires installed on the forklift. A dedicated tire property file for the Elite XP 10.00 - 20.00/8.00 solid tires should be prepared.
- The multibody model does not include driver module and is based on providing steering input directly to the tires. In future, a driver module which follows a given trajectory can be investigated for the rear-wheel steered forklift.
- To validate the multibody model with the static ISO 22915 stability platform tests, initial steps were taken using the MF tire force and torque block which decreased the user involvement and gave promising results. However, when the tires lift off the ground, the force on the tire contact patch should decrease to zero. This phenomenon is not modeled and there may exist a tire force after the wheels lift off from the ground. This is not studied in detail and needs attention in the future.
- Flexible bodies play an important role in the ISO 22915 verification of stability tests. Therefore, the mast in the front end equipment can be modeled as a flexible body.
- The multibody model is functional for reverse driving by providing a negative velocity. This results in a negative throttle pedal position as output from the cruise controller which is not realistic. In future, a realistic reverse driving model can be included.
- Currently the measured signals are filtered with a zero phase filter in MATLAB to reduce noise. Therefore, the quality of the measured signals can be improved.

References

[1] *Forklift Safety Statistics*. 2021. eprint: https://www.safetyinnumbers.ca/wp-content/uploads/2018/04/Forklift-Accident-Statistics-2018.pdf.

[2] *Industrial Trucks - Verification of Stability - Part 2 - Counterbalanced Trucks with Mast*. ISO 22915-2, 2018.

[3] M. Emam, M. Marzouk, and S. Shaaban, "A monitoring device of forklift's stability triangle," *Mobility and Vehicle Mechanics*, vol. 43, pp. 13–27, Jul. 2017.

[4] WWRPManual, *Stability Theory for Forklifts*. Hyster-Yale Group Nederland B.V., 2022.

[5] P. Nikolaou, *Master Thesis - Dynamic Load Detection*. HAN University of Applied Sciences, 2020.

[6] A. Martini, G. Bonelli, and A. Rivola, "Virtual testing of counterbalance forklift trucks: Implementation and experimental validation of a numerical multibody model," *Machines*, vol. 8, p. 26, May 2020.

[7] M. Gardella and A. Martini, "Multibody models and simulations to assess the stability of counterbalance forklift trucks," in Jan. 2020, pp. 526–533.

[8] N. V. D. Wouw, *Multibody and Non Linear Dynamics: Lecture Notes and Exercise*. Eindhoven University of Technology, 2021.

[9] S. Baaij, *Development and validation of a multibody model of a Renault Twizy*. Eindhoven University of Technology, Jan. 2019.

[10] C. J. Ven, *Investigating the possibilities of a flexible manipulator in Amesim to predict reaction forces*. University of Twente, Jun. 2023.

[11] I. Besselink, A. J. Schmeitz, and H. B. Pacejka, "An improved Magic Formula/swift tyre model that can handle inflation pressure changes," *Vehicle System Dynamics*, pp. 337–352, 2010.

[12] M. van Es, *Development of a torque steer analysis tool for electric vehicles [DC.2022.102]*. Eindhoven University of Technology, Dec. 2022.

[13] S. Backhuijs, *Development and validation of a multibody model of the Lupo 3L and EL [DC.2020.074]*. Eindhoven University of Technology, Aug. 2020.

[14] J. W. Loof, *PhD Thesis : Modeling and control of a truck steering-system for active driver support*. Eindhoven University of Technology, Feb. 2018.

[15] T. J. Larsson and G. Rechnitzer, "Forklift trucks—analysis of severe and fatal occupational injuries, critical incidents and priorities for prevention," *Safety Science*, vol. 17, no. 4, pp. 275–289, 1994.

[16] Y. Hou, "Roll and yaw stability evaluation of class 8 trucks with single and dual trailers in low-and high-speed driving conditions," Ph.D. dissertation, Virginia Tech, 2017.

[17] Z. Jin, J. Li, Y. Huang, and A. Khajepour, "Study on rollover index and stability for a triaxle bus," *Chinese Journal of Mechanical Engineering*, vol. 32, Dec. 2019.

[18] B.-C. Chen and H. Peng, "Differential-braking-based rollover prevention for sport utility vehicles with human-in-the-loop evaluations," *Vehicle System Dynamics*, vol. 36, no. 4-5, pp. 359–389, 2001.

[19] B. T. Railsback and R. M. Ziernicki, "Stand-up forklift acceleration," in *ASME International Mechanical Engineering Congress and Exposition*, vol. 44489, 2010, pp. 421–424.

[20] C. Smith, *Chapter 5: Steering Geometry and Self Steering Efforts, Tune to Win: The art and science of race car development and tuning*. SAE International, 1978.

[21] I. Besselink, *Vehicle Dynamics – 4AT000 : Single track vehicle model*. Eindhoven University of Technology, 2021.

[22] I. Besselink, T. Veldhuizen, and H. Nijmeijer, "Improving yaw dynamics by feedforward rear wheel steering," in *2008 IEEE Intelligent Vehicles Symposium*, 2008, pp. 246–250.

[23] *Road Vehicles - Vehicle Dynamics and Road Holding Ability*. ISO 8855, 2011.

[24] G. R. Miller, "The effect of Ackerman steering correction upon front tire wear of medium duty trucks," *SAE International*, p. 12, Nov. 1986.

[25] G. vam Kempen, *Multi-body modelling of the Lupo 3L and EL: system modelling and validation [DC.2019.025]*. Eindhoven University of Technology, Feb. 2019.

[26] K. Čulík, A. Kalašová, and V. Štefancová, "Evaluation of driver's reaction time measured in driving simulator," *Sensors*, vol. 22, pp. 13–27, May 2022.

[27] *Safety of Inductrial Trucks - Dynamic tests for verification of lateral stability - counterbalanced trucks with mast*. EN ISO 16203:2016, 2016.

Appendix A

Model Simulation guide

The multibody forklift model is developed in MATLAB Simulink (version 2022b) with the additional Simscape Multibody package (version 5.3).

As mentioned in Section 4.1, the process to run the multibody model consists of three steps namely: pre-processing, simulation and post-processing. Pre-processing is the process of loading all the truck parameters in MATLAB and defining all input signals and initial conditions. Subsequently, the actual simulation is executed. As a part of post-processing, the correlation coefficients are calculated and desired graphs are generated. These three processes are conducted after running one of the commands in the MATLAB script `Lift_Truck_ToDo.m`. This is the main script which has the possibility to run the scenarios by executing the commands written in the script. Each command triggers different functions depending on the scenario to be simulated.

For example, one of the command in the script is:

```
run_Straight('LFT_Model2_ISOwP',300,0,15);
```

This command triggers the function '`run_straight`' whose name denotes the scenario which has to be simulated. This function has a number of inputs as seen from the command, starting with the model name which is '`LFT_Model2_ISOwP`'. The second input is the fork height which is specified as '`300` mm'. The next input is the mast inclination angle which is set to '`0` degree'. The last input for this function is the vehicle velocity given as '`15` km/h'. Similar to this, other scenarios have a separate function file in which specific inputs are provided. The scenarios available are:

1. Straight
2. Corner (Left or right can be specified)
3. Straight line braking
4. Steady state circle
5. Reverse Corner
6. 90 degree turn
7. Stability platform tests (discussed in Section A.1)
8. Dynamic Validation tests (discussed in Section A.2)

A.1 Run: ISO 22915 verification of stability tests

For simulating the ISO 22915: verification of stability tests, two different approaches have been developed. Each approach has a separate multibody model and can be simulated with the commands mentioned in the main script.

An example of how to simulate the two approaches consisting of different models is provided below:

```
run_StabilityTest1('LFT_Model2_ISOwP_PlatformTest_ExtForce',4750,0,3.60,0);
```

The above listed command is used to simulate the ISO 22915 forward stability: test 1 from the approach 2 using MF tire block. The function name '`run_StabilityTest1`' denotes the stability test which is simulated. The inputs to this function are same as before consisting of model name, fork height, mast inclination angle. In addition, the platform angle is also added as input to be specified in degrees. Since these are static tests, the velocity is removed as an input and in place of velocity, the steering angle is added. In this example, the last input denotes the steering angle specified as '0' degree.

The model named '`LFT_Model2_ISOwP_PlatformTest_ExtForce`' uses the MF tire force and torque block to simulate the ISO 22915 stability platform tests. The model named '`LFT_Model2_ISOwP_PlatformTest_BushingJoint`' uses the bushing joints to simulate the same. All the other inputs apart from the model name are same for both the approaches. After simulating a specific scenario or a stability platform test, the user can generate plots from the scripts named: '`Tireplot.m`' and '`Stability_Platform_Test_Plots.m`'.

A.2 Run: Dynamic validation tests

The dynamic validation tests performed on the forklift H9XD6 are simulated by providing certain inputs to the MATLAB multibody model from the truck CAN bus. Therefore, a separate function named '`run_DynamicValidation`' is developed to simulate these tests. An example for simulating one of the dynamic validation tests is shown below:

```
run_DynamicValidation('LFT_Model2_ISOwP',500,0,3,"SteadyState_Left.csv");
```

As mentioned, the function to simulate the dynamic validation tests requires certain inputs to be simulated. The common inputs are the model name, fork height, mast inclination angle and initial velocity as specified earlier. However, in order to provide input such as the reference velocity profile, brake pedal position and steering cylinder displacement, a `.csv` file is required. This file contains all the data which has been logged from the test. By selecting the respective column number, '`run_DynamicValidation`' first extracts the required inputs from the `.csv` file and then filters them before starting the simulation. Once all the inputs are gathered and filtered, the simulation starts and takes approximately the same amount of time as in reality.

After the simulation is completed, the output signals are saved in the MATLAB base workspace. The script named '`TestDataAnalysis`' is used to filter the output signals extracted from the `.csv` file and also plot the respective signals for comparison. In order to calculate the correlation coefficients between the two measured signals, the script '`ResultQuantification.m`' is used.

Appendix B

Accelerometer modelling

This chapter presents the in depth validation of the gravitational correction performed on the acceleration outputs of the transform sensor block in Simscape multibody to represent the results obtained with an accelerometer. Section 5.3.2 discusses the solution of the research performed by Baaij [9], where the gravitational acceleration component ($\vec{g}$) dependent on the orientation of the sensor is added to the inertial acceleration ($\vec{a}$) measured by the transform sensor in Simscape. By this addition, acceleration measured by the vehicle accelerometer ($\vec{f}$) is obtained.

Before implementing the solution expressed by (5.2) to the main forklift multibody model, this correction is first tried and tested on a simple model. A simple multibody model representing a car making a steady state circle at constant angular velocity is developed. Figure B.1 represents the mechanism implemented in the MATLAB environment where R is the turning radius, r is the yaw velocity (constant in this case) and m is the vehicle mass. The transform sensor is located at the center of the body represented by the red circle.

Considering the vehicle mass $m = 1200$ kg is running at constant yaw velocity $r = 1.385$ rad/s following the steady state circle of radius $R = 3$ m, would experience certain constant lateral acceleration (a_y) and a gravitational acceleration. The lateral acceleration can be given by the following expression:

$$a_y = \frac{V^2}{R} = \omega^2 \cdot R \tag{B.1}$$

The expected lateral acceleration calculated by (B.1) and the gravitational acceleration without a roll angle developed should be: $a_{y,\text{sensor}} = 5.76$ m/s^2 & $a_{z,\text{sensor}} = 9.80665$ m/s^2

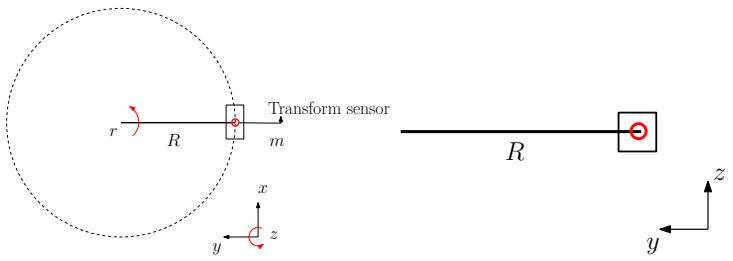

(a) Top view **(b)** Side view

Figure B.1: Multibody mechanism developed in MATLAB

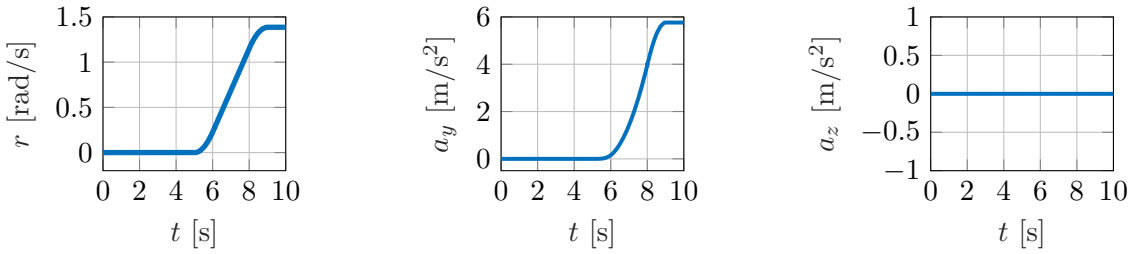

(a) Yaw velocity **(b)** Lateral acceleration **(c)** Vertical acceleration

Figure B.2: Outputs of a tranform sensor block

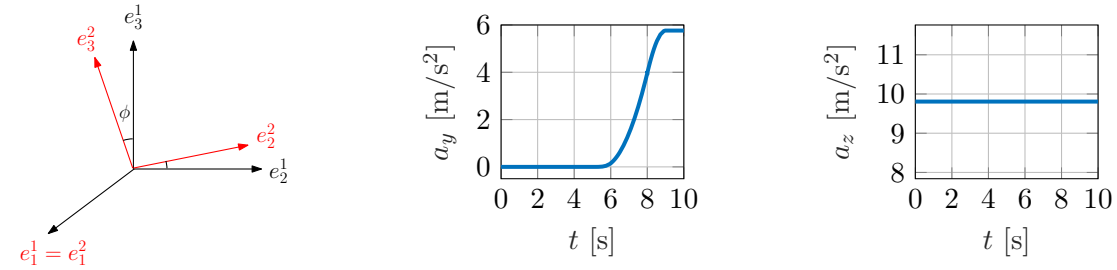

(a) Frame transformation **(b)** Lateral acceleration **(c)** Vertical acceleration

Figure B.3: Outputs after modeling the accelerometer

This simple implementation is done in MATLAB and the angular velocity shown in Figure B.2a is provided as input to the mechanism. As seen the angular velocity is maintained constant at $r = 1.385$ rad/s towards the end of the simulation. At constant angular velocity, the expected lateral acceleration calculated by (B.1) should be equal to 5.76 m/s^2 which is also depicted in Figure B.2b. However, the vertical acceleration given by the transform sensor is shown in Figure B.2c, which is equal to 0 m/s^2. Observing this, it is concluded that the transform sensor output in Simscape needs correction to match the output given by the accelerometer situated on the actual vehicle.

Therefore, the solution in the form of (5.2) and (5.3) given by Baaij [9] is implemented in Simscape. The rotation matrix can be derived by the transformation concepts [8]. If a body is rotated by an angle ϕ with respect to the first axis, the body will be oriented as shown in Figure B.3a by the red frames. Hence, by frame transformations the rotation matrix is given as:

$$e^2 = R^* \cdot e^1$$

$$R^* = \begin{bmatrix} 1 & 0 & 0 \\ 0 & \cos(\phi) & \sin(\phi) \\ 0 & -\sin(\phi) & \cos(\phi) \end{bmatrix}$$

By implementing the solution shown in (5.3), the vertical acceleration calculated by (B.2) represents the acceleration sensed by the accelerometer on the vehicle.

$$a_{z,\text{IMU}} = a_{z,\text{sensor}} - \cos(\phi) \cdot g, \tag{B.2}$$

where $a_{z,\text{IMU}}$ is the acceleration sensed by the accelerometer, $a_{z,\text{sensor}}$ is the acceleration sensed by transform sensor, ϕ is the roll angle and g is the gravitational acceleration. Since the roll angle (ϕ) is equal to 0 in this situation, the acceleration equals 9.80665 m/s^2 shown in Figure B.3c. Furthermore, the lateral acceleration after this correction, shown in Figure

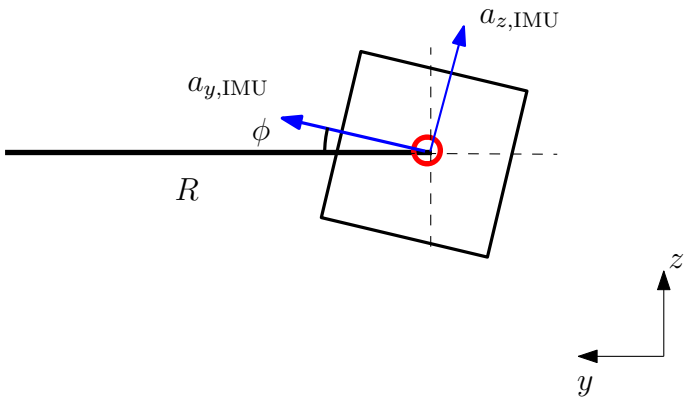

Figure B.4: Effect of roll angle (ϕ)

B.3b remains same which should be the case as the roll angle is 0.

Considering, the vehicle is taking a left hand turn, the effect of roll angle will be significant. Assuming the vehicle develops a roll angle (ϕ) of magnitude 7 degrees, the multibody mechanism is subjected to a roll angle as shown in Figure B.4. The roll angle is negative as the moment due to the load transfer is in clockwise direction. In this case, the lateral acceleration sensed by the accelerometer can be calculated by (B.3) which has an influence of the roll angle. The gravitational acceleration will also decrease as the body is tilted and can be calculated by (B.2).

$$a_{y,\text{IMU}} = a_{y,\text{sensor}} - (-\sin(\phi)(g)) \tag{B.3}$$

The values obtained for the accelerations sensed by the accelerometer in the y and z directions are 6.94 m/s^2 and 9.73 m/s^2, respectively.

These values are validated by the developed simple multibody model and it is concluded that the solution implemented corrects the output of the transform sensor in Simscape. After implementing this solution, the outcome can be compared to the accelerations measured by the real vehicle accelerometer referred to as IMU sensors in this thesis.

Appendix C

Multibody model validation results

This chapter presents the validation results for the ISO 22915: verification of stability tests and the steady state right turn test.

C.1 ISO 22915: verification of stability

The remaining test results apart from the stability test 1 explained in Section 5.2, are presented in this section. Figure C.1 depicts the platform tilt angle with respect to time for the stability test 2. It can be observed that approach 2 involving the MF tire force and torque block provides a better prediction which is more close to the WWRP prediction as compared to the approach 1 involving bushing joints.

Analysis of CoG position in the stability triangle
Figure C.2 presents the CoG positions shown inside the stability triangle of the lift truck H9XD6. Similar to test 1, it is evident in test 2 also that as the platform starts to tilt and reaches the respective angle at which the truck initiates to top over, the CoG is near to the stability boundary.

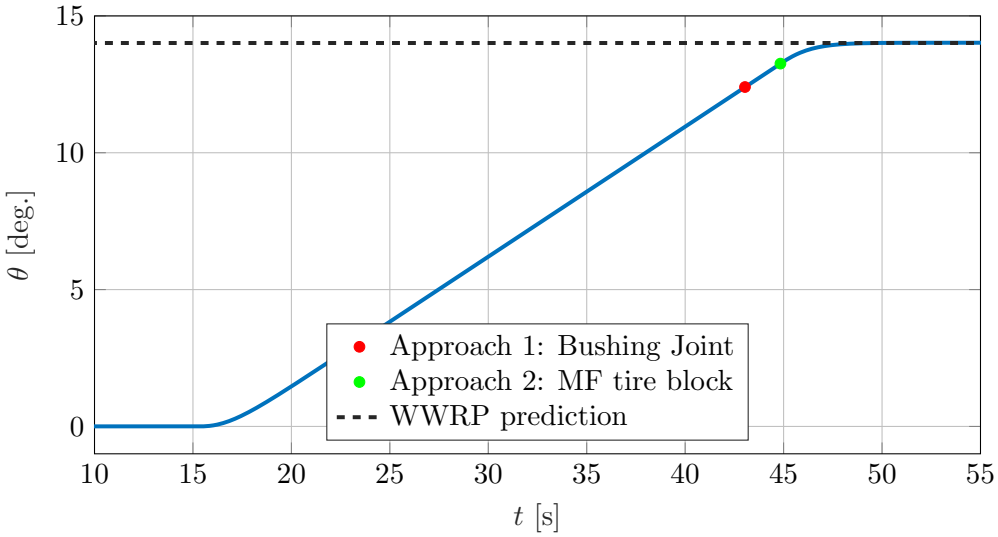

Figure C.1: ISO stability test 2: platform tilt angle

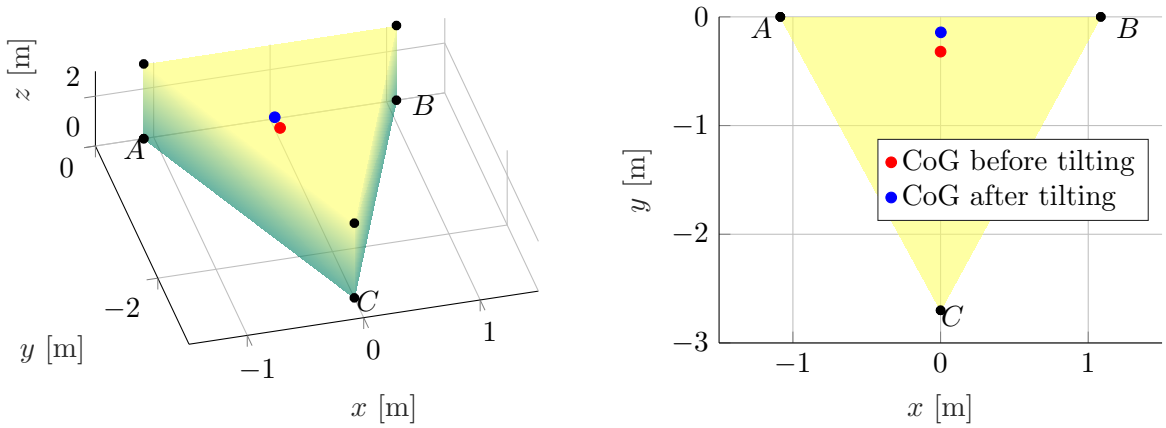

Figure C.2: ISO stability test 2: CoG position in stability triangle

Similar results have been obtained for test 3 and test 4 which are summarised below:

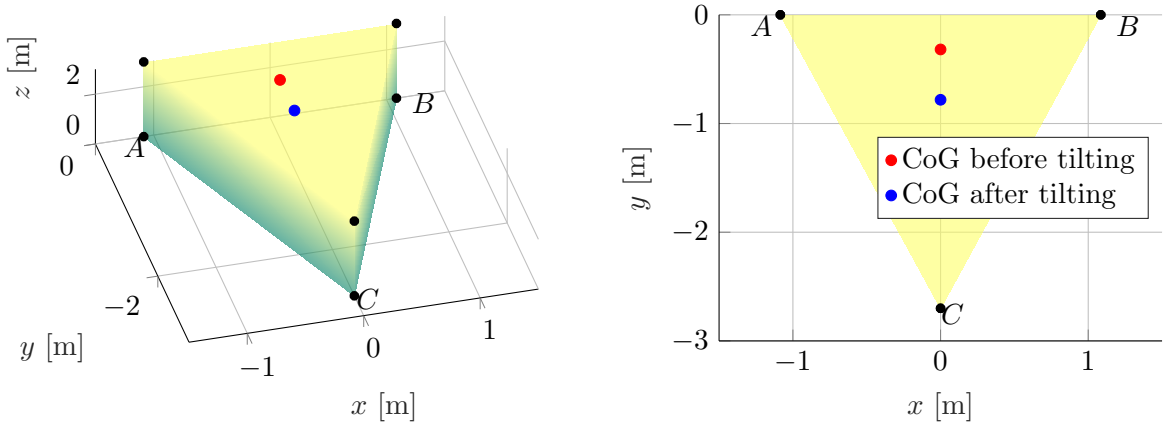

Figure C.3: ISO stability test 3: CoG position in stability triangle

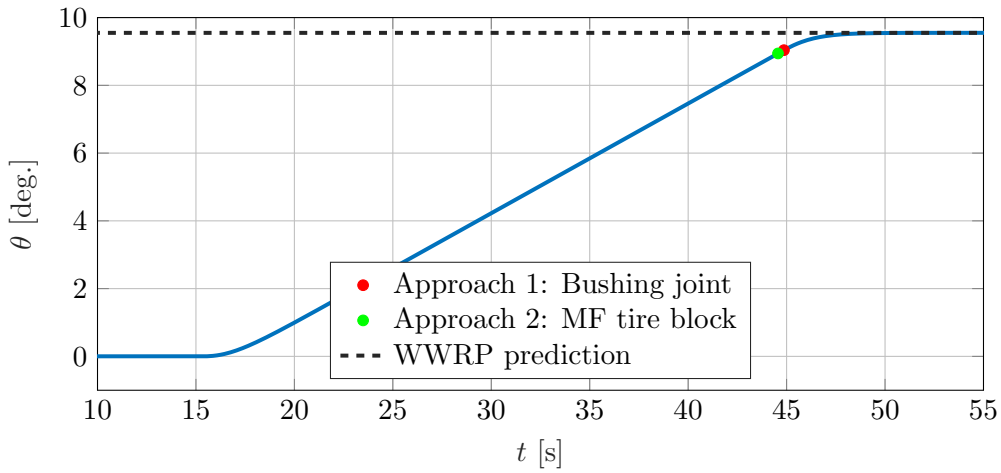

Figure C.4: ISO stability test 3: platform tilt angle

Figure C.3 presents the location of CoG before and after tilting the platform for stability test 3. This test accounts for lateral stability and is terminated when the front outer tire looses contact with the ground. In the test 3, the truck does not reach its stability limit. This is indicated by the CoG position in Figure C.3, where it can be seen that the CoG is not yet close to the boundary and is well inside the stability triangle as the truck has not reached its stability limit.

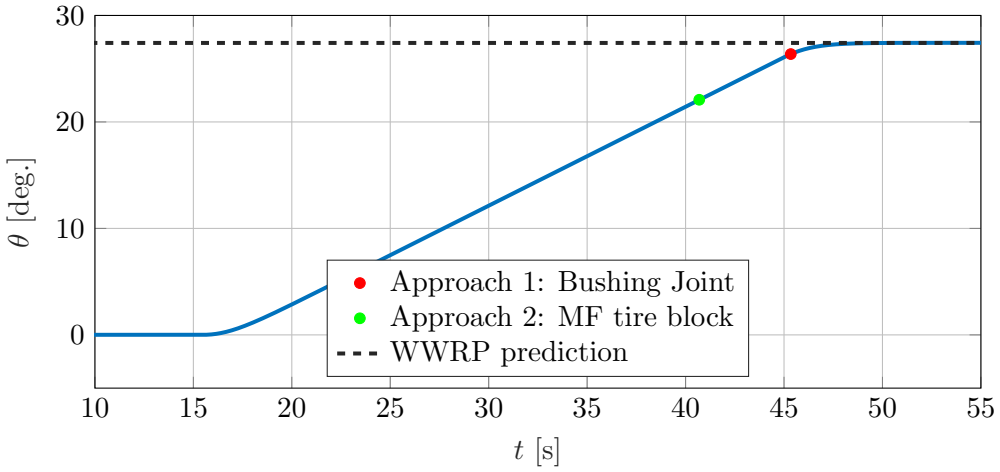

Figure C.5: ISO stability test 4WL: platform tilt angle

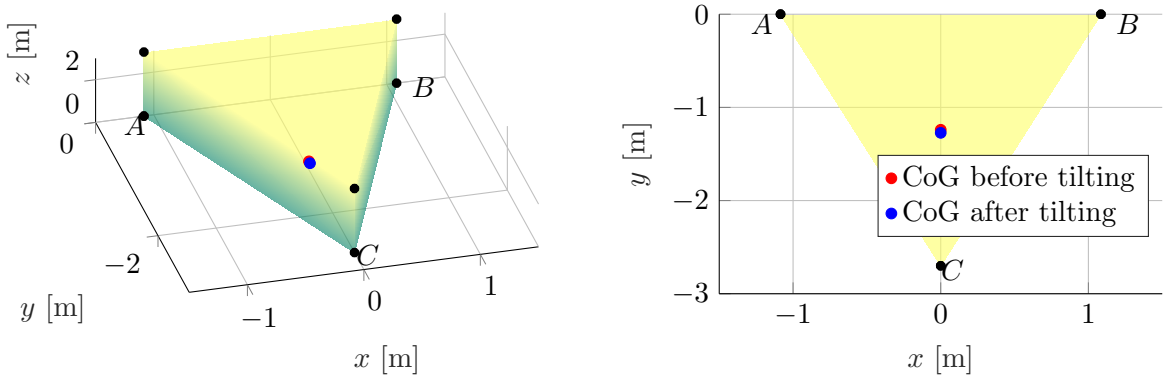

Figure C.6: ISO stability test 4WL: CoG position in stability triangle

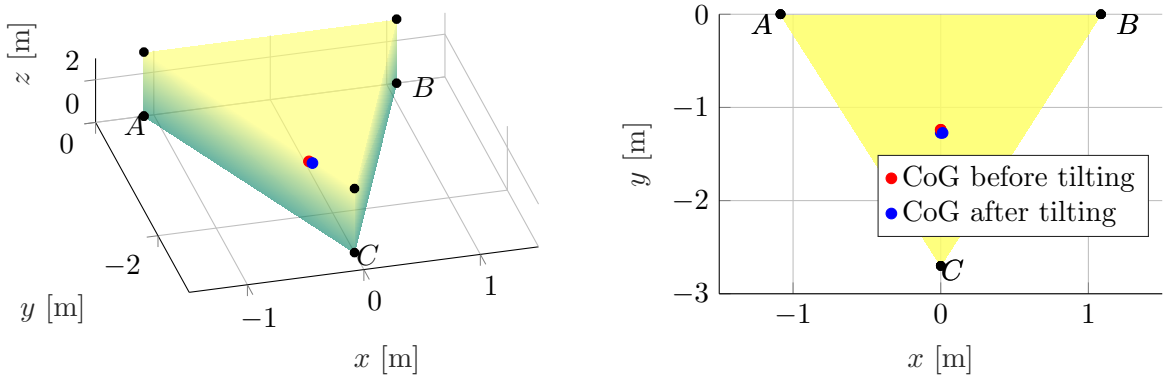

Figure C.7: ISO stability test 4ULT: CoG position in stability triangle

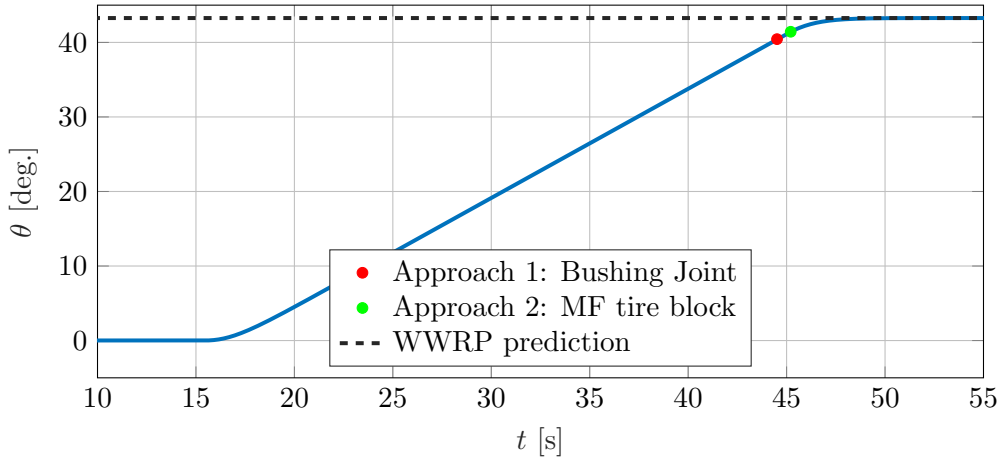

Figure C.8: ISO stability test 4ULT: platform tilt angle

Figures C.5 and C.6 represent the results for the lateral stability test 4 WL which is terminated as soon as the front outer tire looses contact with the ground. On the other hand, Figure C.7 and C.8 depict the results for test 4 ULT which is terminated when the complete truck rolls over.

As stated in Chapter 2, for steady state situations the truck is predicted to be stable only if the resultant force acting on the CoG meets the ground inside the stability triangle boundary. There can be possibility that the CoG is inside the stability boundary but the truck still tips or rolls over as the resultant force on the CoG meets the ground outside the stability boundaries. This is seen in Figure C.7. The CoG is nowhere close to the stability triangle boundary but the truck has still rolled over. Therefore, looking only at the CoG position of the truck and ensuring that it is inside the stability triangle does not account for stability.

C.2 Steady-state circular driving: right turn

The results of the steady-state dynamic test for a left turn are explained in Section 5.3.4. In addition, similar steady-state turning tests were also conducted for a right turn following the same procedure. Figure C.9 shows the obtained results from the right-turn steady-state circular driving test. It is observed that the magnitude of the output signals is approximately equal, however, the sign is obviously opposite. The yaw rate has a negative sign according to the ISO 8855 sign convention when the truck is turning right. Table C.1 presents the correlation coefficients for the steady-state circular driving test for a right hand turn.

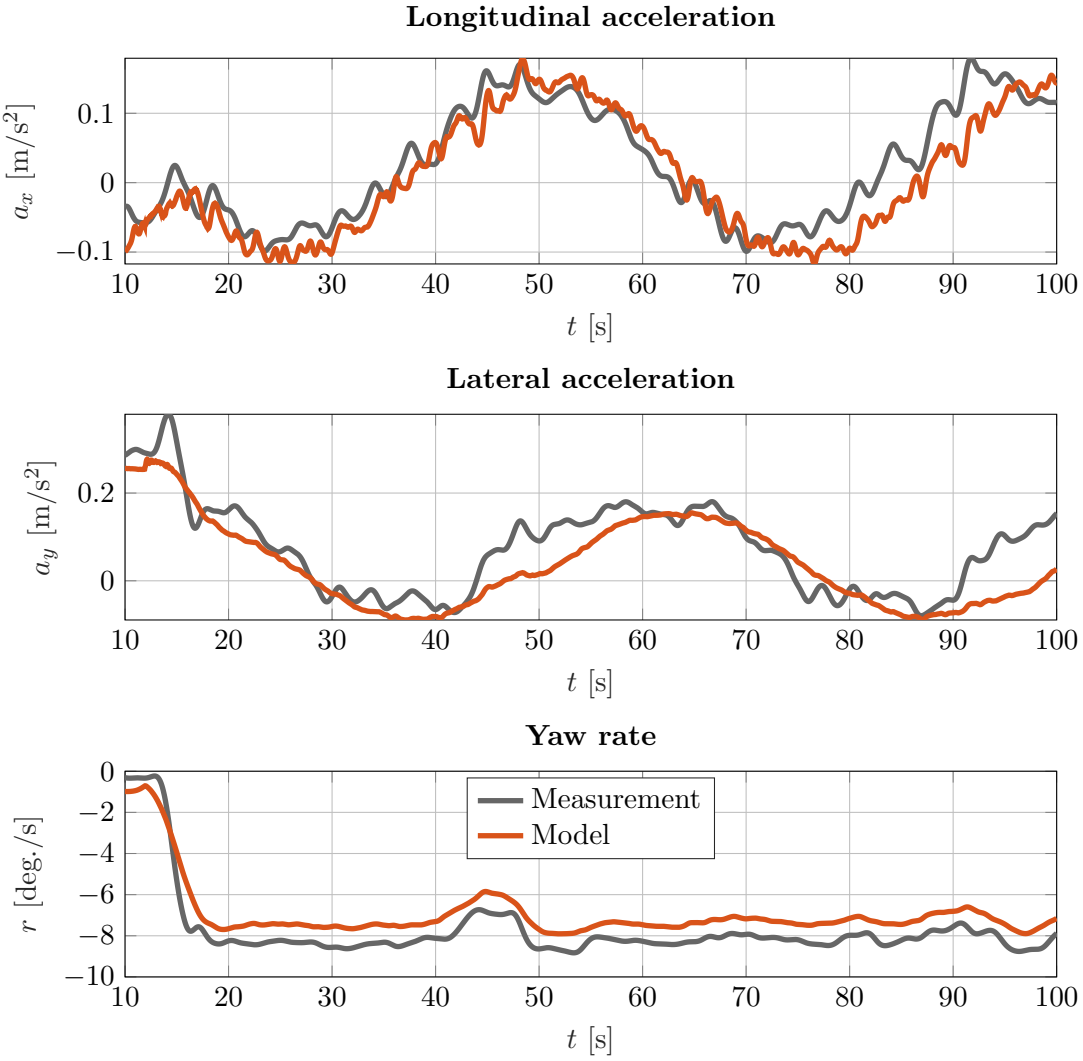

Figure C.9: Steady-state circular driving: right turn results

Table C.1: Steady-state circular driving (right turn): correlation coefficients

Signal	R	ϵ	NRMSD
Velocity (V_x)	0.98	0.03	0.06
Longitudinal acceleration (a_x)	0.86	2.5	0.09
Lateral acceleration (a_y)	0.76	4.2	0.12
Yaw rate (r)	0.92	33	0.33